US 20190019630A1

(19) United States

(12) Patent Application Publication (10) Pub. No.: US 2019/0019630 A1

Strauss et al. (43) Pub. Date: Jan. 17, 2019

(54) **SIMPLE ROUTE TO HIGHLY CONDUCTIVE POROUS GRAPHENE FROM CARBON NANODOTS FOR SUPERCAPACITOR APPLICATIONS**

(71) Applicant: **The Regents of the University of California**, Oakland, CA (US)

(72) Inventors: **Volker Strauss**, Los Angeles, CA (US); **Richard B. Kaner**, Pacific Palisades, CA (US); **Maher F. El-Kady**, Los Angeles, CA (US)

(21) Appl. No.: **16/033,266**

(22) Filed: **Jul. 12, 2018**

Related U.S. Application Data

(60) Provisional application No. 62/532,684, filed on Jul. 14, 2017.

Publication Classification

(51) **Int. Cl.**

H01G 11/36	(2006.01)
C01B 32/184	(2006.01)
H01G 11/24	(2006.01)
H01G 11/86	(2006.01)

(52) **U.S. Cl.**

CPC ***H01G 11/36*** (2013.01); ***C01B 32/184*** (2017.08); *B82Y 30/00* (2013.01); ***H01G 11/86*** (2013.01); ***H01G 11/24*** (2013.01)

(57) **ABSTRACT**

Disclosed herein are methods and compositions directed to a promising class of nanomaterials called organic nanoparticles, or carbon nanodots. The present disclosure provides a facile method for the conversion of biomolecule-based carbon nanodots into high surface area three-dimensional graphene networks with excellent electrochemical properties.

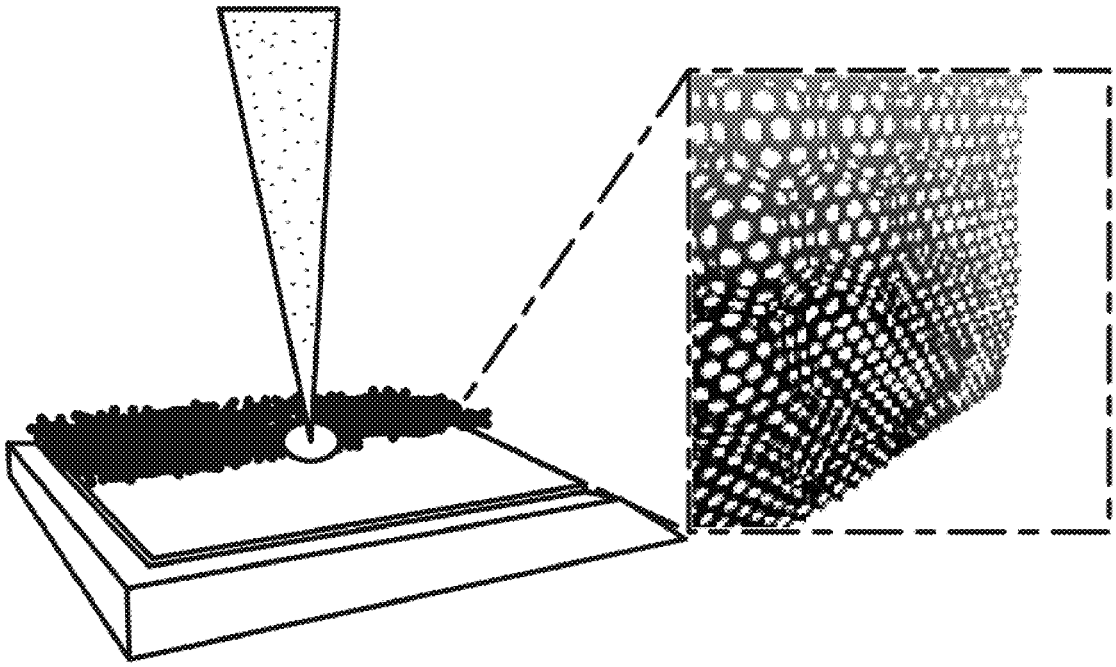

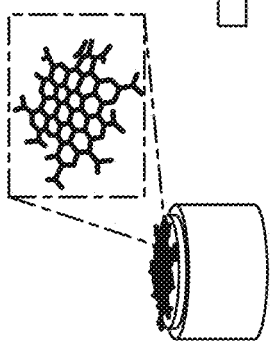

FIG. 1A

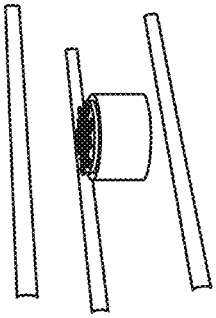

FIG. 1B

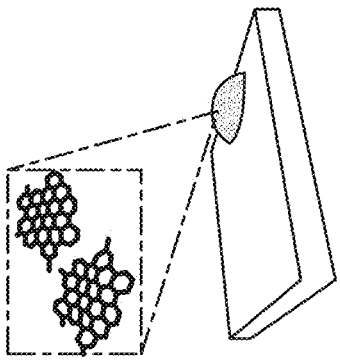

FIG. 1C

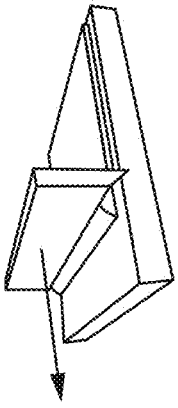

FIG. 1D

FIG. 1E

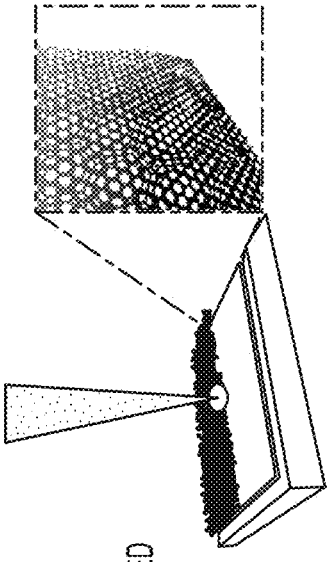

FIG. 1F

FIG. 2

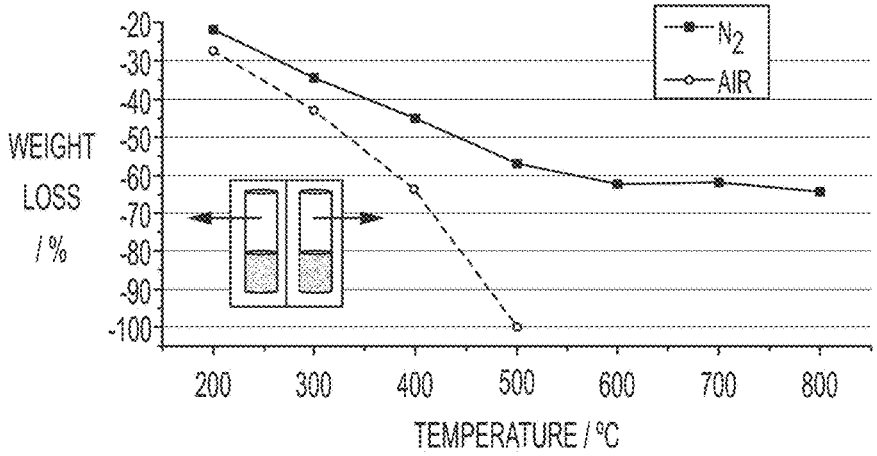
WEIGHT LOSS / %
-20
-30
-40
-50
-60
-70
-80
-90
-100
200
300
400
500
600
700
800
TEMPERATURE / °C
N2
AIR

FIG. 3A

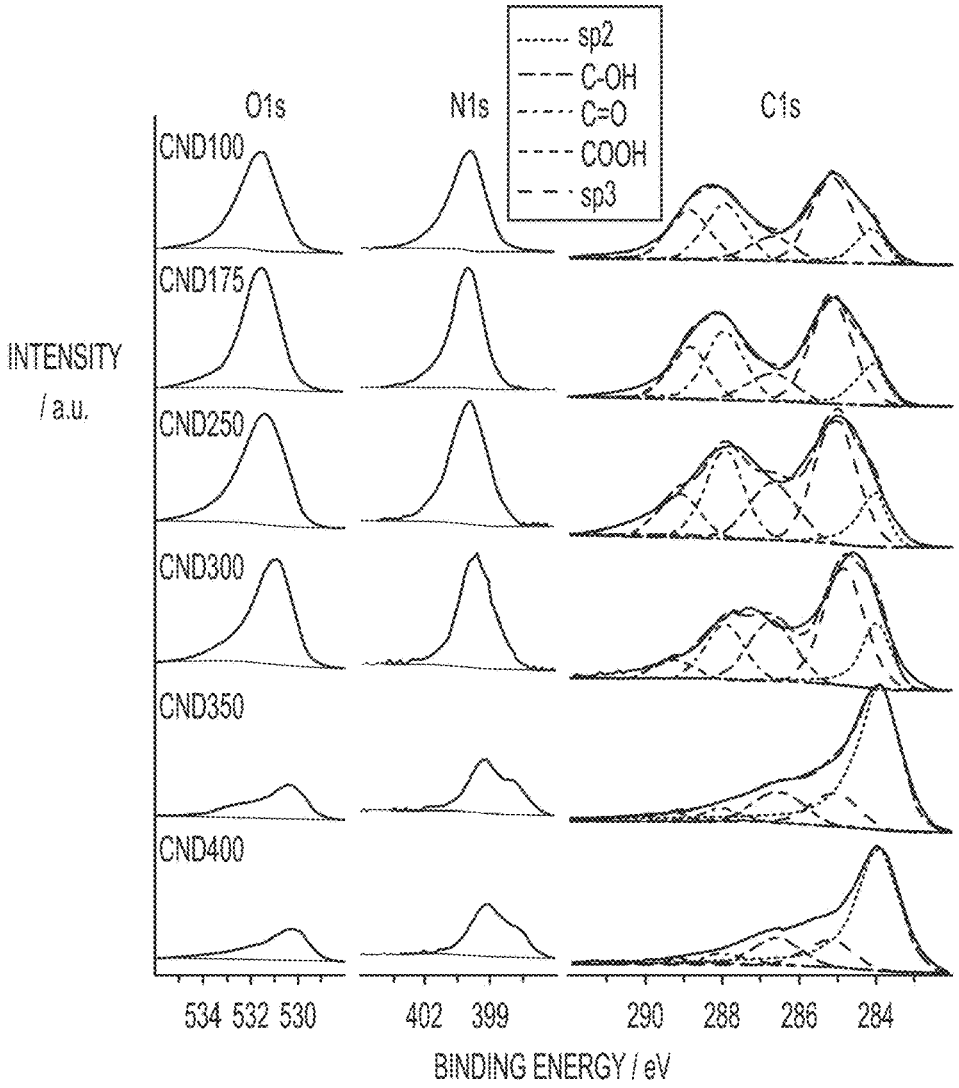
O1s
N1s
C1s
sp2
C-OH
C=O
COOH
sp3
CND100
CND175
CND250
CND300
CND350
CND400
INTENSITY / a.u.
534 532 530
402 399
290 288 286 284
BINDING ENERGY / eV

FIG. 3B

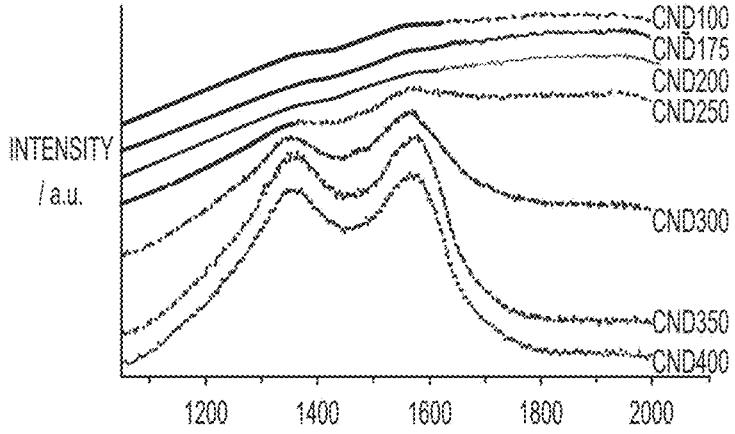

FIG. 3C

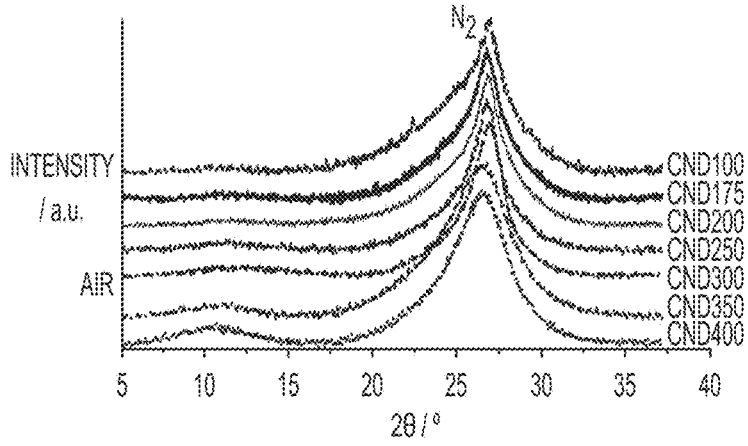

FIG. 3D

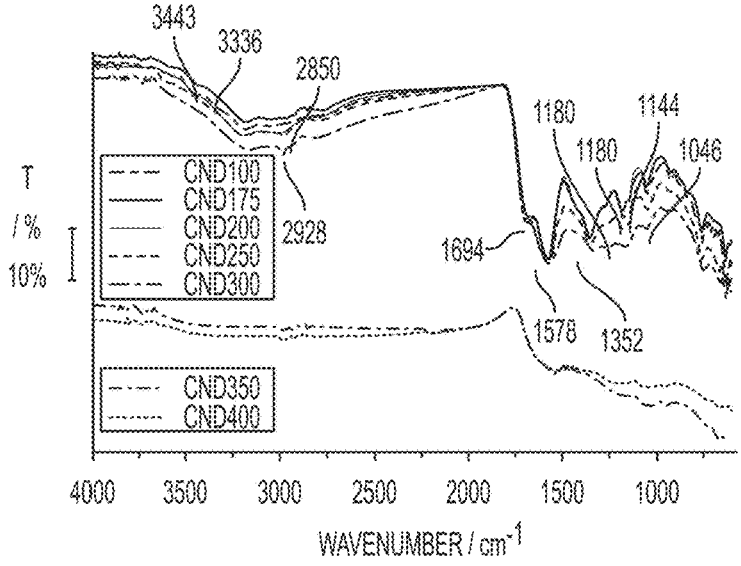

FIG. 3E

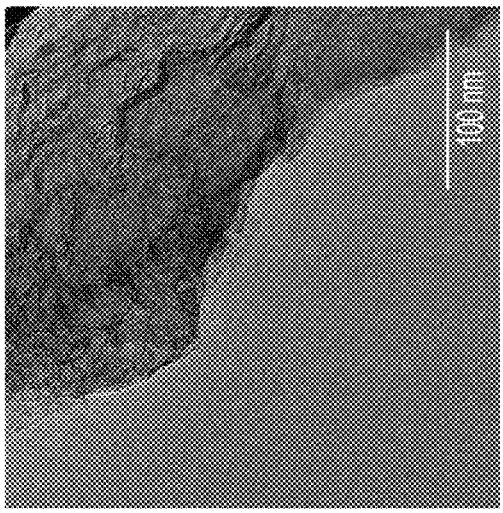

FIG. 4C

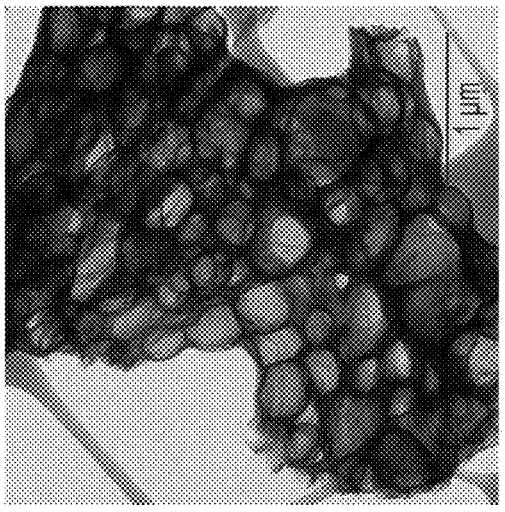

FIG. 4B

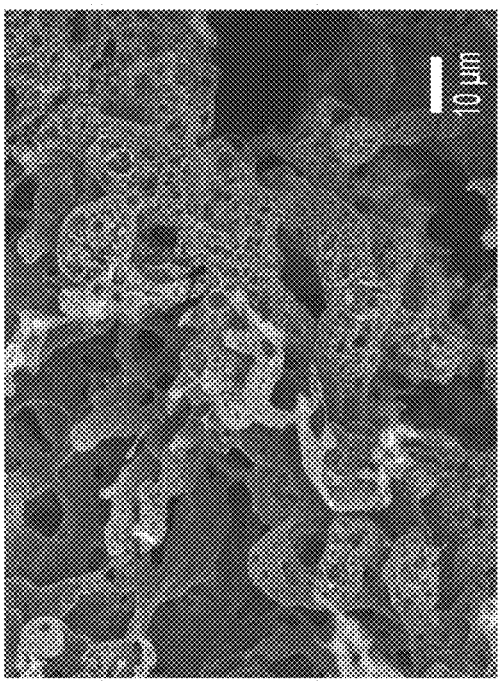

FIG. 4A

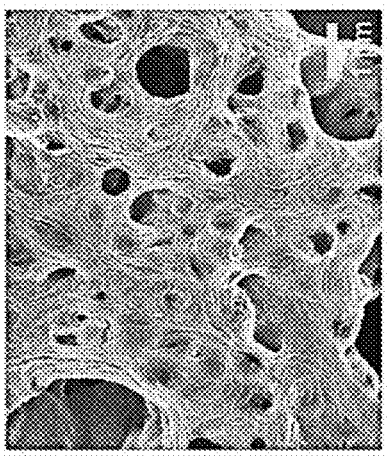

FIG. 5C

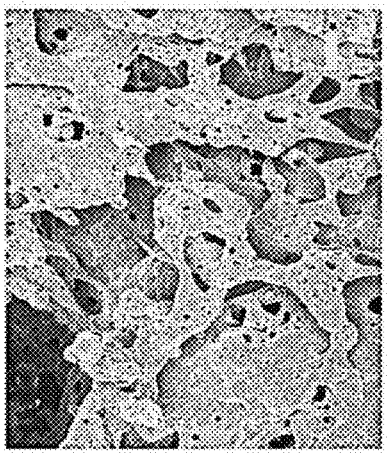

FIG. 5B

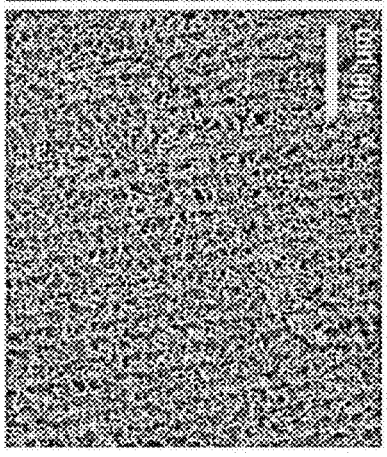

FIG. 5A

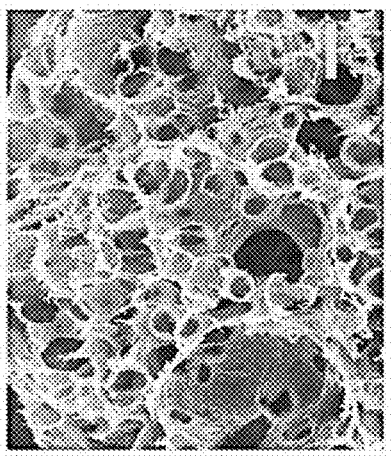

FIG. 5F

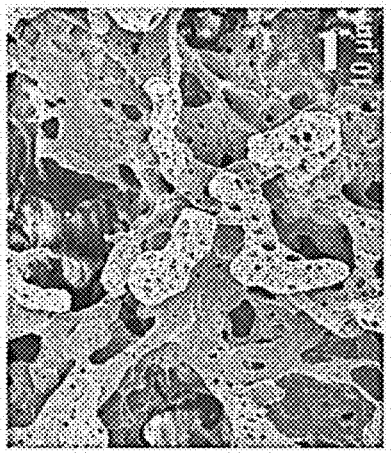

FIG. 5E

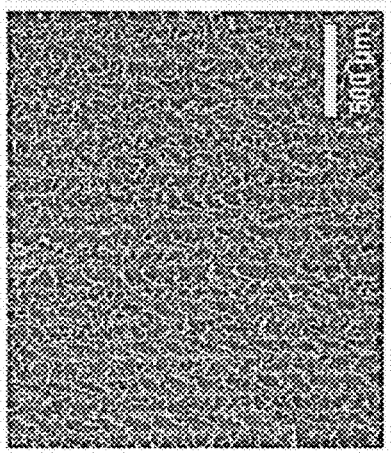

FIG. 5D

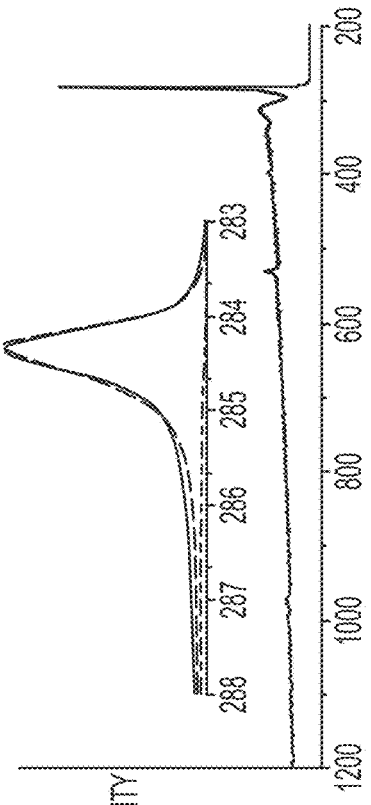
INTENSITY / a.u.
1200
1000
800
600
400
200
WAVENUMBERS / cm-1
288
287
286
285
284
283

FIG. 6B

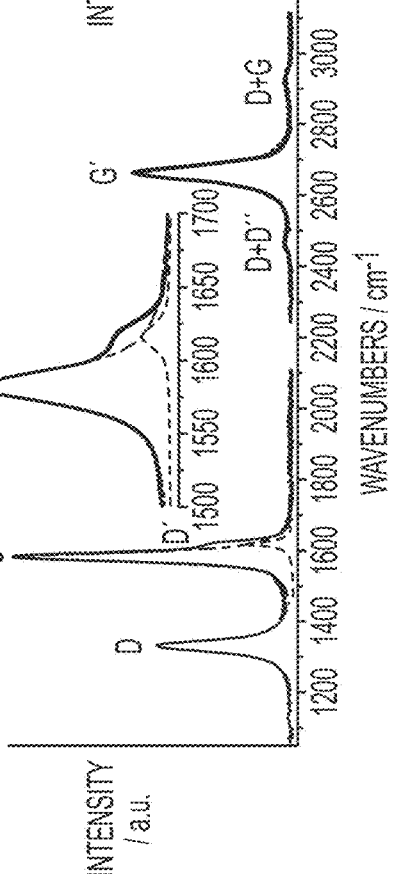
INTENSITY / a.u.
G
D
D'
G'
D+D''
D+G
1200
1400
1600
1800
2000
2200
2400
2600
2800
3000
1500
1550
1600
1650
1700
WAVENUMBERS / cm-1

FIG. 6A

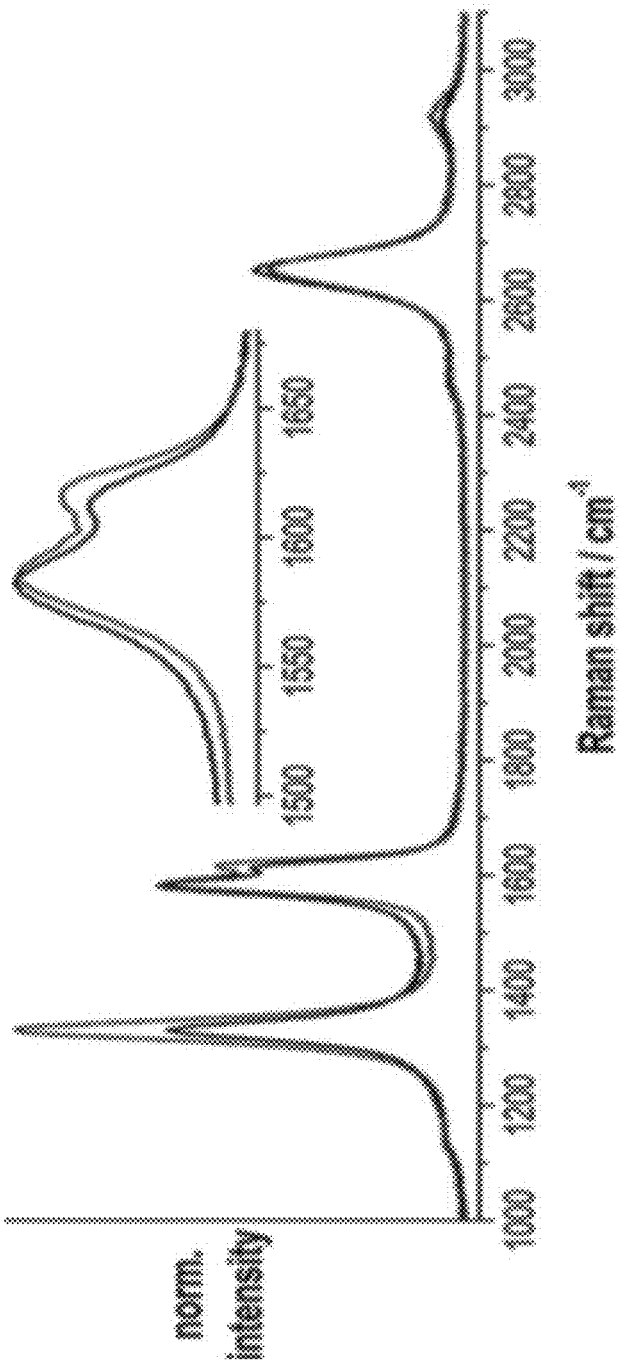
norm. intensity
1000
1200
1400
1600
1800
2000
2200
2400
2600
2800
3000
Raman shift / cm-1
1500
1550
1600
1650

FIG. 7

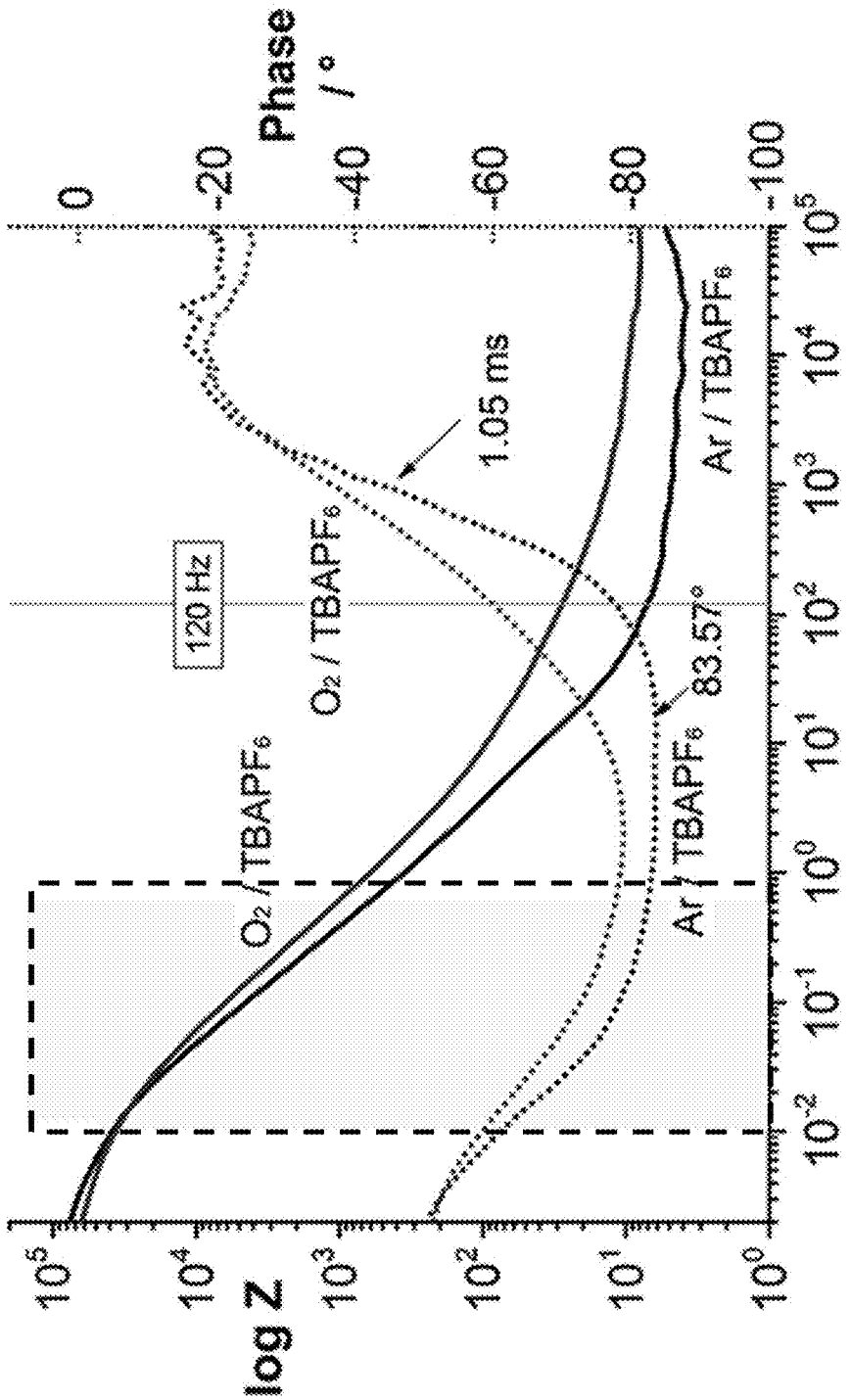
Phase / °
0
-20
-40
-60
-80
-100
log Z
log f
120 Hz
1.05 ms
83.57°
O2 / TBAPF6
Ar / TBAPF6

FIG. 8

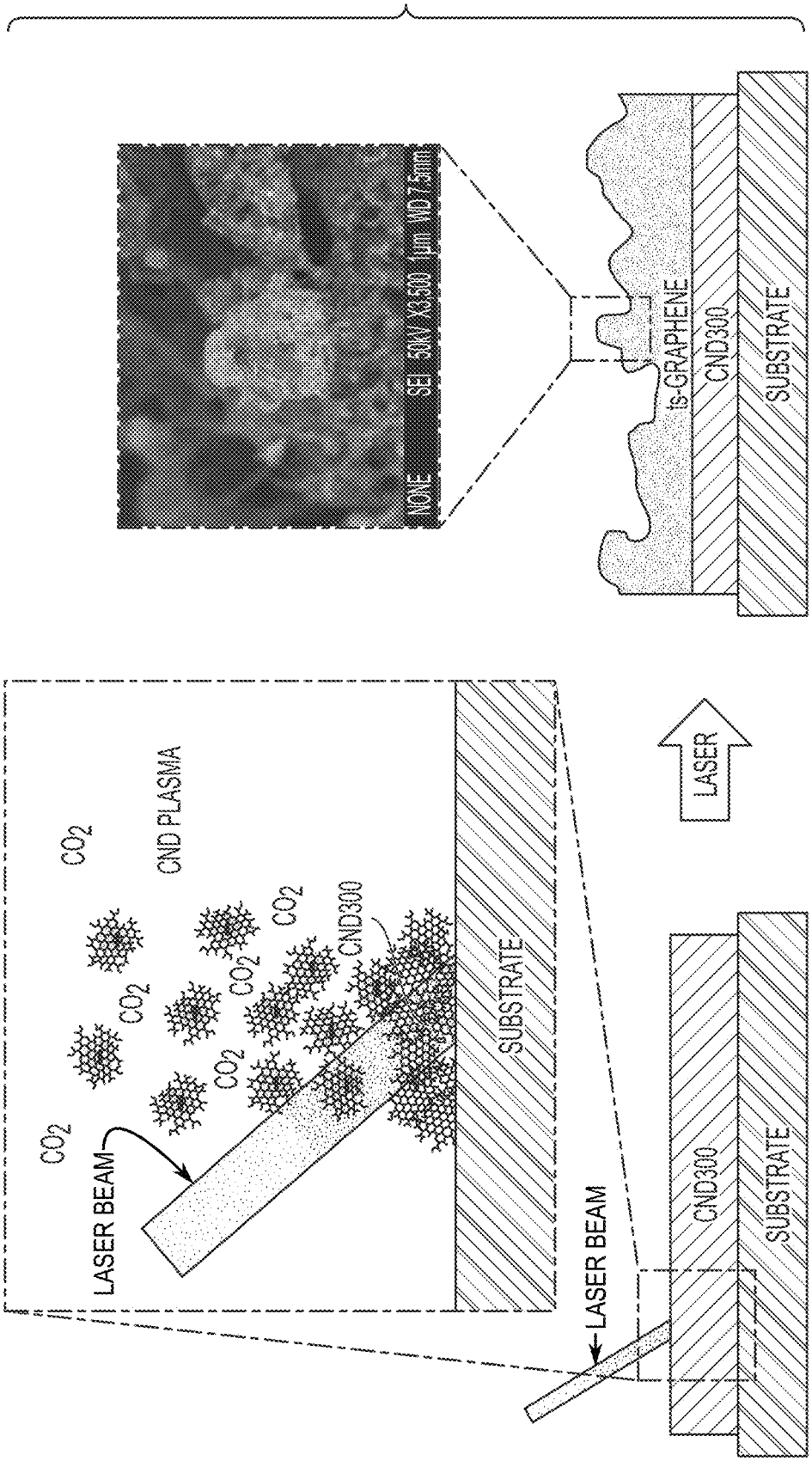
NONE SEI 30kV X3,500 1μm WD 7.5mm
ts-GRAPHENE
CND300
SUBSTRATE
CND PLASMA
CO_2
LASER BEAM
LASER
SUBSTRATE
CND300
SUBSTRATE
LASER BEAM

FIG. 9

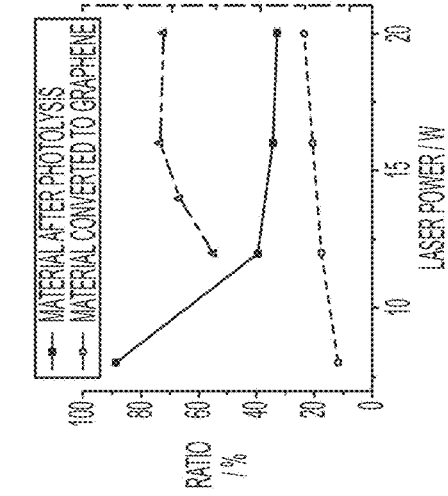

FIG. 10A

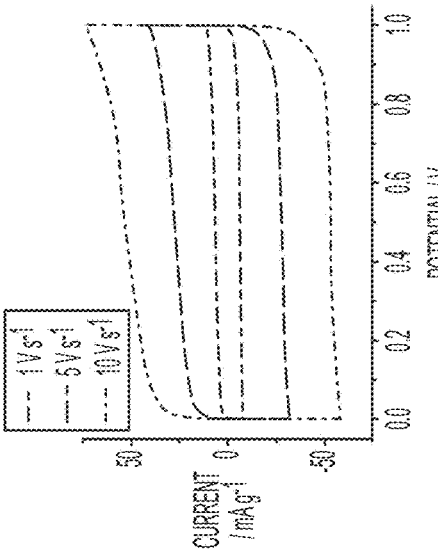

FIG. 10B

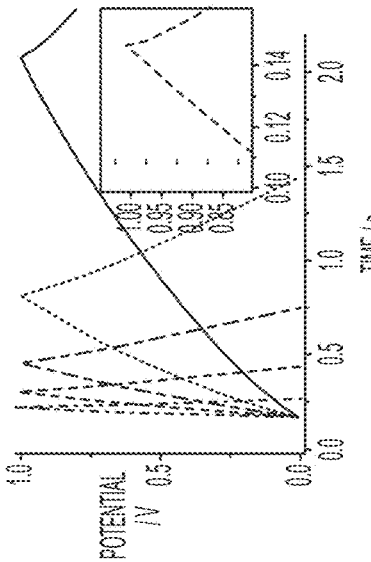

FIG. 10C

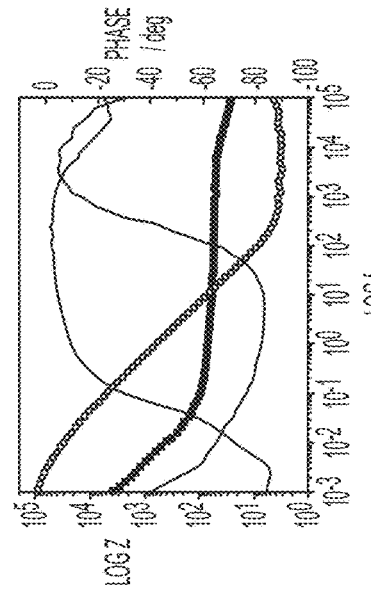

FIG. 10F

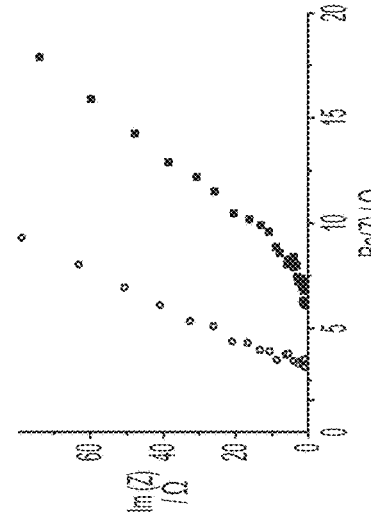

FIG. 10E

FIG. 10D

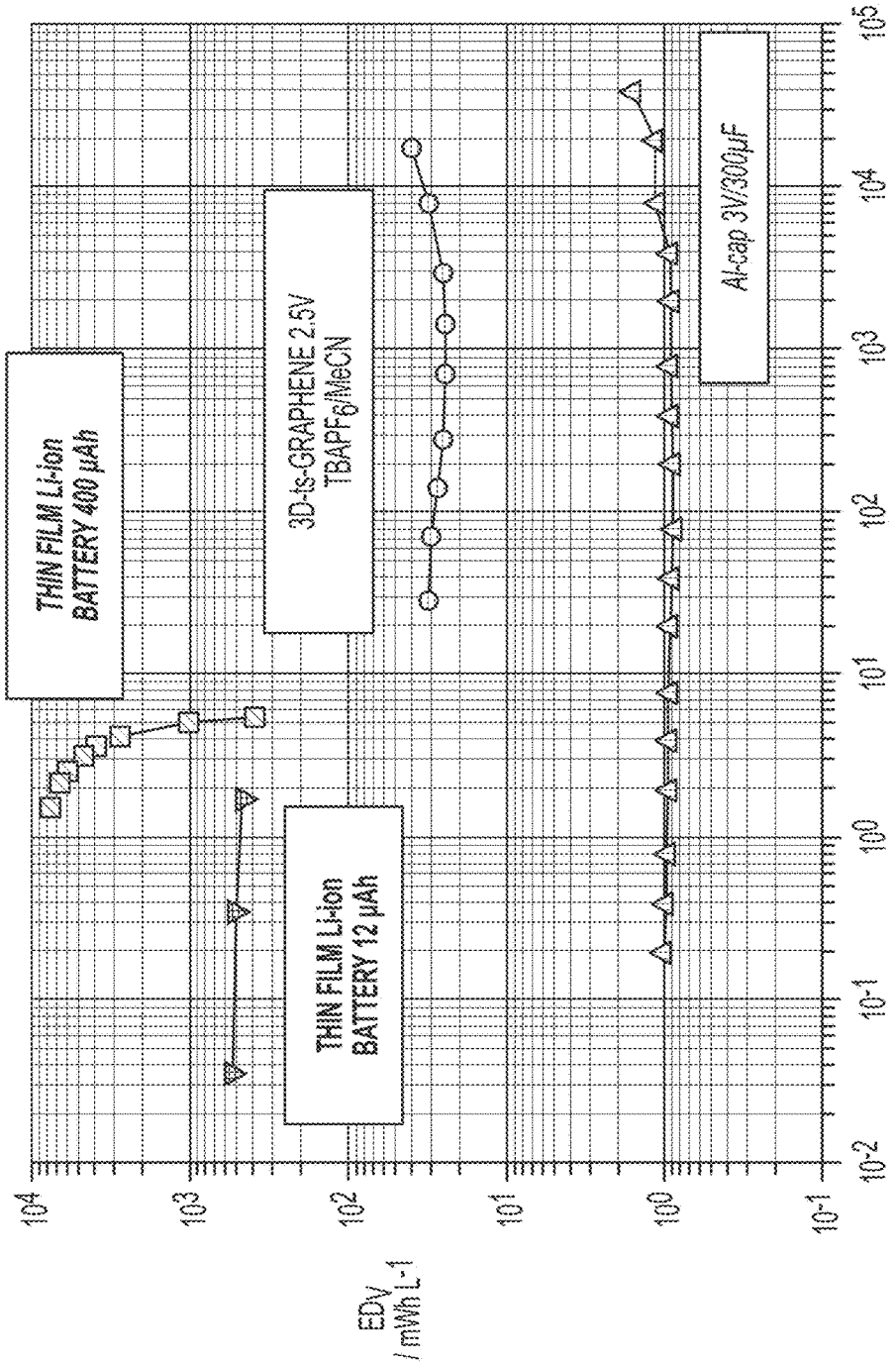
THIN FILM Li-ion
BATTERY 400 µAh
3D-ts-GRAPHENE 2.5V
TBAPF6/MeCN
Al-cap 3V/300µF
THIN FILM Li-ion
BATTERY 12 µAh
EDV / mWh L-1
PDV / W L-1
10-2
10-1
100
101
102
103
104
105

FIG. 11

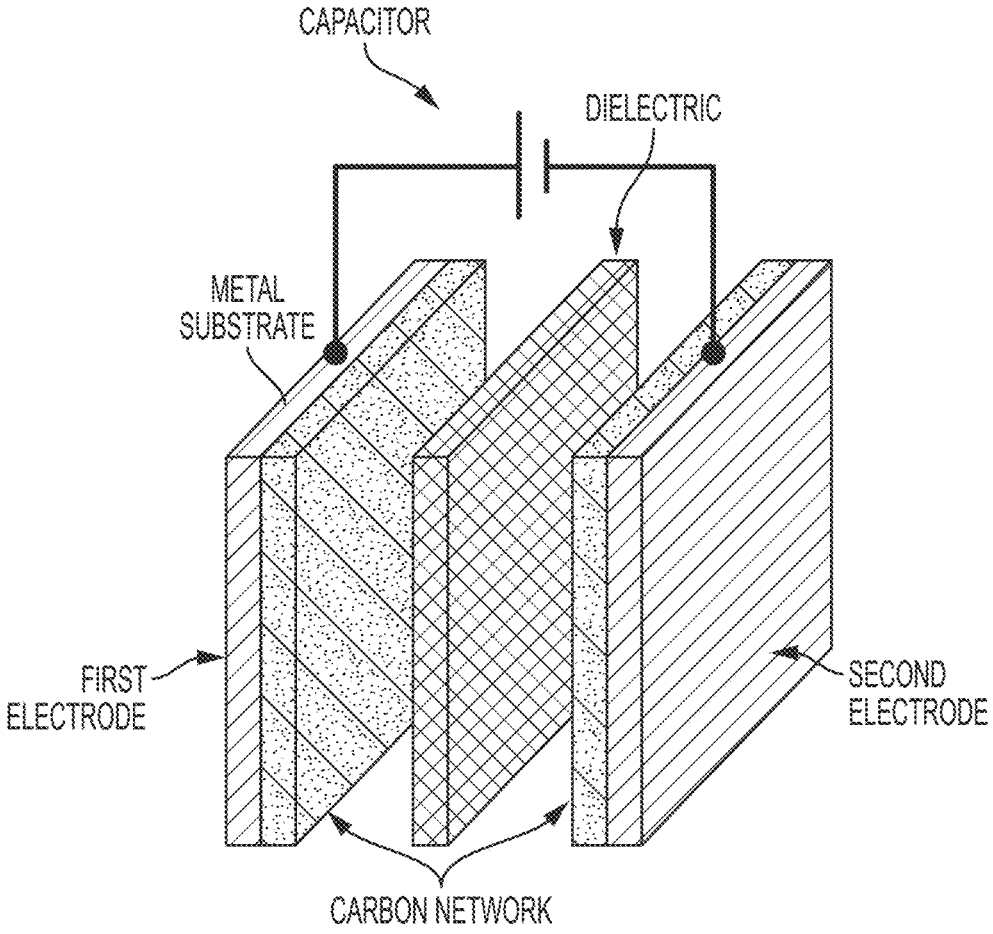
CAPACITOR
DIELECTRIC
METAL SUBSTRATE
FIRST ELECTRODE
SECOND ELECTRODE
CARBON NETWORK

FIG. 12

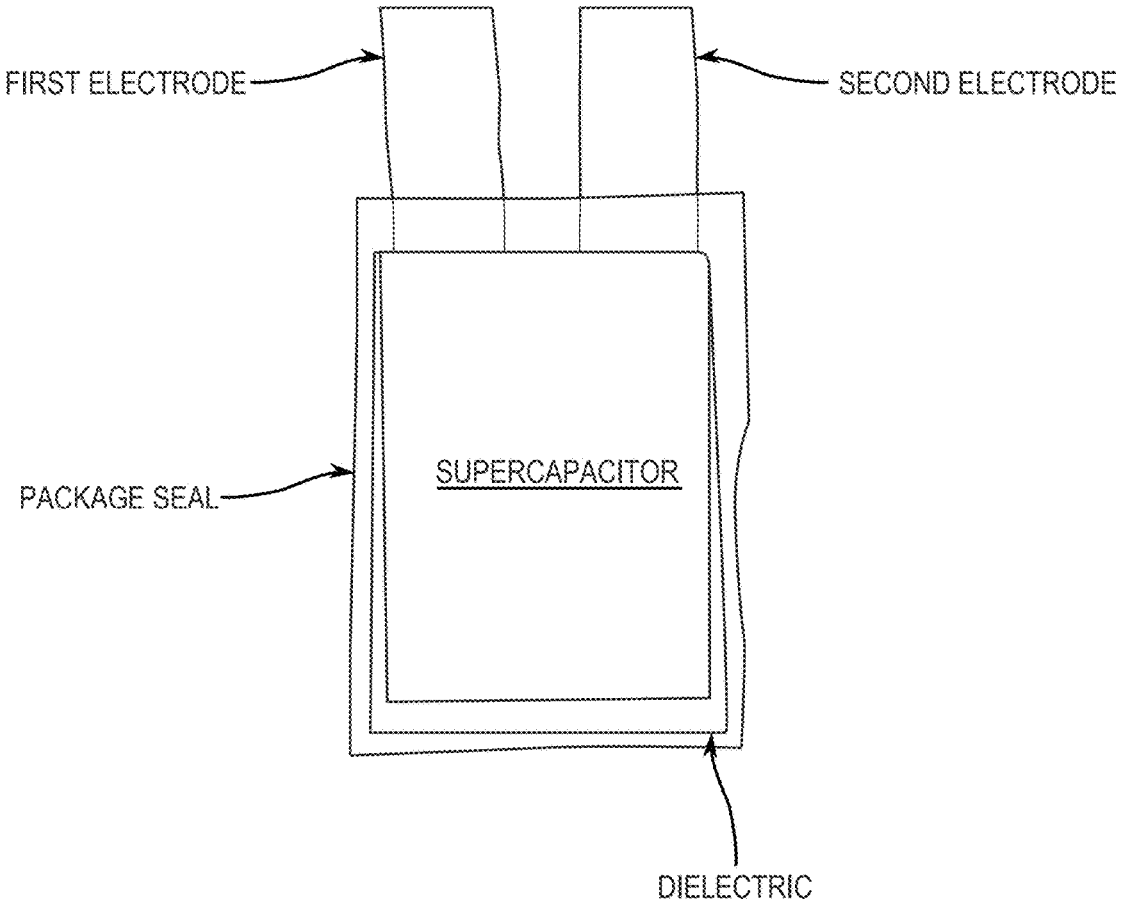
FIRST ELECTRODE
SECOND ELECTRODE
PACKAGE SEAL
SUPERCAPACITOR
DIELECTRIC

FIG. 13

SIMPLE ROUTE TO HIGHLY CONDUCTIVE POROUS GRAPHENE FROM CARBON NANODOTS FOR SUPERCAPACITOR APPLICATIONS

BACKGROUND

[0001] The global energy supply is one of the biggest issues facing materials science and technology. For the transition from fossil fuels to renewables, major improvements in current technology and investigation of new materials are essential.

SUMMARY

[0002] Disclosed herein are methods and compositions directed to a promising class of nanomaterials called organic nanoparticles, or carbon nanodots (CNDs), which have multiple applications in fields ranging from optoelectronics to biomedicine. The present disclosure provides a facile method for the conversion of biomolecule-based CNDs into high surface area three-dimensional graphene networks with excellent electrochemical properties.

[0003] In some embodiments, CNDs are prepared by either oxidative cutting of larger graphitic carbons or carbonization of amorphous precursors. Carbonization of amorphous precursors transforms amorphous carbon to graphitic carbon using various biomaterials and biomolecules containing a high amount of oxidized groups. Key electrochemical properties of CNDs can be altered by controlling the conditions during the carbonization process, such as temperature and pressure, and selecting a suitable precursor.

[0004] It is recognized herein that the tunable and optimal morphological and electronic properties of CNDs, such as surface area, crystalline domains, and charge trapping centers, enable use of CNDs as electroactive components in energy storage devices such as electrochemical capacitors, supercapacitors, batteries, hybrid supercapacitors, and pseudocapacitors. Although CNDs have intrinsically low electrical conductivity and complex electrochemical behavior that may hinder their direct application in supercapacitors, their abundance of surface functional groups enables a multitude of modifications and reactions. As an example, in some embodiments, thermal treatment (thermolysis) is used to enable the modification of such material properties or conversion into graphene by light or laser irradiation. Moreover, as CNDs contain a graphitic/graphenic core to form smaller homologues of graphene, they can be used as precursors for larger extended π-systems.

[0005] Provided herein is a carbon network comprising turbostratic graphene. In some embodiments, the carbon network comprising turbostratic graphene has an active surface area of at least about 230 square meters per gram (m^2/g). In some embodiments, the carbon network comprising turbostratic graphene has an active surface area of at least about 100 m^2/g, at least about 120 m^2/g, at least about 140 m^2/g, at least about 160 m^2/g, at least about 180 m^2/g, at least about 200 m^2/g, at least about 220 m^2/g, at least about 240 m^2/g, at least about 260 m^2/g, at least about 280 m^2/g, or at least about 300 m^2/g. In some embodiments, the carbon network comprising turbostratic graphene has an electrical conductivity of at least about 200 siemens per meter (S/m). In some embodiments, the carbon network comprising turbostratic graphene has an electrical conductivity of at least about 100 S/m, at least about 120 S/m, at least about 140 S/m, at least about 160 S/m, at least about 180 S/m, at least about 200 S/m, at least about 220 S/m, at least about 240 S/m, at least about 260 S/m, at least about 280 S/m, or at least about 300 S/m.

[0006] In some embodiments, the porous carbon network has an average pore size of about 10 nm to about 100,000 nm. In some embodiments, the porous carbon network has an average pore size of at least about 10 nm. In some embodiments, the porous carbon network has an average pore size of at most about 100,000 nm. In some embodiments, the porous carbon network has an average pore size of about 10 nm to about 50 nm, about 10 nm to about 100 nm, about 10 nm to about 500 nm, about 10 nm to about 1,000 nm, about 10 nm to about 5,000 nm, about 10 nm to about 10,000 nm, about 10 nm to about 50,000 nm, about 10 nm to about 100,000 nm, about 50 nm to about 100 nm, about 50 nm to about 500 nm, about 50 nm to about 1,000 nm, about 50 nm to about 5,000 nm, about 50 nm to about 10,000 nm, about 50 nm to about 50,000 nm, about 50 nm to about 100,000 nm, about 100 nm to about 500 nm, about 100 nm to about 1,000 nm, about 100 nm to about 5,000 nm, about 100 nm to about 10,000 nm, about 100 nm to about 50,000 nm, about 100 nm to about 100,000 nm, about 500 nm to about 1,000 nm, about 500 nm to about 5,000 nm, about 500 nm to about 10,000 nm, about 500 nm to about 50,000 nm, about 500 nm to about 100,000 nm, about 1,000 nm to about 5,000 nm, about 1,000 nm to about 10,000 nm, about 1,000 nm to about 50,000 nm, about 1,000 nm to about 100,000 nm, about 5,000 nm to about 10,000 nm, about 5,000 nm to about 50,000 nm, about 5,000 nm to about 100,000 nm, about 10,000 nm to about 50,000 nm, about 10,000 nm to about 100,000 nm, or about 50,000 nm to about 100,000 nm. In some embodiments, the porous carbon network has an average pore size of about 10 nm, about 50 nm, about 100 nm, about 500 nm, about 1,000 nm, about 5,000 nm, about 10,000 nm, about 50,000 nm, or about 100,000 nm. In some embodiments, the porous carbon network has an average pore size of at least about 10 nm, at least about 50 nm, at least about 100 nm, at least about 500 nm, at least about 1,000 nm, at least about 5,000 nm, at least about 10,000 nm, at least about 50,000 nm, or at least about 100,000 nm. In some embodiments, the porous carbon network has an average pore size of no more than about 10 nm, no more than about 50 nm, no more than about 100 nm, no more than about 500 nm, no more than about 1,000 nm, no more than about 5,000 nm, no more than about 10,000 nm, no more than about 50,000 nm, or no more than about 100,000 nm.

[0007] In some embodiments, the carbon network has a Raman spectrum with D-, G-, D', and G'-bands at about 1323 cm^{-1}, about 1570 cm^{-1}, about 1604 cm^{-1}, and about 2636 cm^{-1}. In some embodiments, the carbon network further comprises an amorphous carbon structure having a Raman spectrum with a D band at about 1324 cm^{-1}. In some embodiments, the carbon network further comprises an amorphous carbon structure having a Raman spectrum with a D** band at about 1468 cm^{-1}. In some embodiments, the carbon network further comprises an amorphous carbon structure having a Raman spectrum with a G bands at about 1574 cm^{-1}. In some embodiments, the carbon network has a G' band spectrum curve with a full width at half maximum of about 74 cm^{-1}. In some embodiments, the carbon network has an elemental composition of about 89% carbon, about 8% oxygen, and nitrogen. In some embodiments, the carbon

network has an elemental composition of about 89% carbon, about 8% oxygen, and about 3% nitrogen. In some embodiments, the carbon network has an elemental composition of 89% carbon, 8% oxygen, and 3% nitrogen. In yet other embodiments, the carbon network has an elemental composition of about 90% carbon, about 8% oxygen, and nitrogen.

[0008] Another aspect provided herein is an energy storage device comprising: a first electrode; and a second electrode separated from the first electrode by a dielectric, wherein at least one of the first electrode and the second electrode comprises a carbon network comprising turbostratic graphene.

[0009] In some embodiments, the energy storage device has an active surface area of at least about 230 m^2/g. In some embodiments, the energy storage device has an active surface area of at least about 100 m^2/g, at least about 120 m^2/g, at least about 140 m^2/g, at least about 160 m^2/g, at least about 180 m^2/g, at least about 200 m^2/g, at least about 220 m^2/g, at least about 240 m^2/g, at least about 260 m^2/g, at least about 280 m^2/g, or at least about 300 m^2/g. In some embodiments, the energy storage device has an electrical conductivity of at least about 200 S/m. In some embodiments, the energy storage device has an electrical conductivity of at least about 100 S/m, at least about 120 S/m, at least about 140 S/m, at least about 160 S/m, at least about 180 S/m, at least about 200 S/m, at least about 220 S/m, at least about 240 S/m, at least about 260 S/m, at least about 280 S/m, or at least about 300 S/m. In some embodiments, the energy storage device has an energy density of about 7.5 watt-hours per kilogram (Wh/kg) at a power density of at least about 860 kilowatts. In some embodiments, the energy storage device has an energy density of at least about 3.0 Wh/kg, at least about 3.5 Wh/kg, at least about 4.0 Wh/kg, at least about 4.5 Wh/kg, at least about 5.0 Wh/kg, at least about 5.5 Wh/kg, at least about 6.0 Wh/kg, at least about 6.5 Wh/kg, at least about 7.0 Wh/kg, at least about 7.5 Wh/kg, at least about 8.0 Wh/kg, at least about 8.5 Wh/kg, or at least about 9.0 Wh/kg at a power density of at least about 800 kW kg^{-1}, at least about 820 kW kg^{-1}, at least about 840 kW kg^{-1}, at least about 860 kW kg^{-1}, at least about 880 kW kg^{-1}, at least about 900 kW kg^{-1}, at least about 920 kW kg^{-1}, at least about 940 kW kg^{-1}, at least about 960 kW kg^{-1}, at least about 980 kW kg^{-1}, or at least about 1000 kW kg^{-1}.

[0010] In some embodiments, the energy storage device has a charge-discharge cycling rate time constant of about 0.5 milliseconds (ms) to about 10 ms. In some embodiments, the energy storage device has a charge-discharge cycling rate time constant of about 0.5 ms to about 0.75 ms, about 0.5 ms to about 1 ms, about 0.5 ms to about 1.5 ms, about 0.5 ms to about 2 ms, about 0.5 ms to about 3 ms, about 0.5 ms to about 4 ms, about 0.5 ms to about 5 ms, about 0.5 ms to about 6 ms, about 0.5 ms to about 8 ms, about 0.5 ms to about 10 ms, about 0.75 ms to about 1 ms, about 0.75 ms to about 1.5 ms, about 0.75 ms to about 2 ms, about 0.75 ms to about 3 ms, about 0.75 ms to about 4 ms, about 0.75 ms to about 5 ms, about 0.75 ms to about 6 ms, about 0.75 ms to about 8 ms, about 0.75 ms to about 10 ms, about 1 ms to about 1.5 ms, about 1 ms to about 2 ms, about 1 ms to about 3 ms, about 1 ms to about 4 ms, about 1 ms to about 5 ms, about 1 ms to about 6 ms, about 1 ms to about 8 ms, about 1 ms to about 10 ms, about 1.5 ms to about 2 ms, about 1.5 ms to about 3 ms, about 1.5 ms to about 4 ms, about 1.5 ms to about 5 ms, about 1.5 ms to about 6 ms, about 1.5 ms to about 8 ms, about 1.5 ms to about 10 ms, about 2 ms to about 3 ms, about 2 ms to about 4 ms, about 2 ms to about 5 ms, about 2 ms to about 6 ms, about 2 ms to about 8 ms, about 2 ms to about 10 ms, about 3 ms to about 4 ms, about 3 ms to about 5 ms, about 3 ms to about 6 ms, about 3 ms to about 8 ms, about 3 ms to about 10 ms, about 4 ms to about 5 ms, about 4 ms to about 6 ms, about 4 ms to about 8 ms, about 4 ms to about 10 ms, about 5 ms to about 6 ms, about 5 ms to about 8 ms, about 5 ms to about 10 ms, about 6 ms to about 8 ms, about 6 ms to about 10 ms, or about 8 ms to about 10 ms. In some embodiments, the energy storage device has a charge-discharge cycling rate time constant of about 0.5 ms, about 0.75 ms, about 1 ms, about 1.5 ms, about 2 ms, about 3 ms, about 4 ms, about 5 ms, about 6 ms, about 8 ms, or about 10 ms. In some embodiments, the energy storage device has a charge-discharge cycling rate time constant of at least about 0.5 ms, at least about 0.75 ms, at least about 1 ms, at least about 1.5 ms, at least about 2 ms, at least about 3 ms, at least about 4 ms, at least about 5 ms, at least about 6 ms, at least about 8 ms, or at least about 10 ms. In some embodiments, the energy storage device has a charge-discharge cycling rate time constant of at most about 0.5 ms, at most about 0.75 ms, at most about 1 ms, at most about 1.5 ms, at most about 2 ms, at most about 3 ms, at most about 4 ms, at most about 5 ms, at most about 6 ms, at most about 8 ms, or at most about 10 ms.

[0011] In some embodiments, the porous carbon network has an average pore size of about 10 nm to about 100,000 nm. In some embodiments, the porous carbon network has an average pore size of at least about 10 nm. In some embodiments, the porous carbon network has an average pore size of at most about 100,000 nm. In some embodiments, the porous carbon network has an average pore size of about 10 nm to about 50 nm, about 10 nm to about 100 nm, about 10 nm to about 500 nm, about 10 nm to about 1,000 nm, about 10 nm to about 5,000 nm, about 10 nm to about 10,000 nm, about 10 nm to about 50,000 nm, about 10 nm to about 100,000 nm, about 50 nm to about 100 nm, about 50 nm to about 500 nm, about 50 nm to about 1,000 nm, about 50 nm to about 5,000 nm, about 50 nm to about 10,000 nm, about 50 nm to about 50,000 nm, about 50 nm to about 100,000 nm, about 100 nm to about 500 nm, about 100 nm to about 1,000 nm, about 100 nm to about 5,000 nm, about 100 nm to about 10,000 nm, about 100 nm to about 50,000 nm, about 100 nm to about 100,000 nm, about 500 nm to about 1,000 nm, about 500 nm to about 5,000 nm, about 500 nm to about 10,000 nm, about 500 nm to about 50,000 nm, about 500 nm to about 100,000 nm, about 1,000 nm to about 5,000 nm, about 1,000 nm to about 10,000 nm, about 1,000 nm to about 50,000 nm, about 1,000 nm to about 100,000 nm, about 5,000 nm to about 10,000 nm, about 5,000 nm to about 50,000 nm, about 5,000 nm to about 100,000 nm, about 10,000 nm to about 50,000 nm, about 10,000 nm to about 100,000 nm, or about 50,000 nm to about 100,000 nm. In some embodiments, the porous carbon network has an average pore size of about 10 nm, about 50 nm, about 100 nm, about 500 nm, about 1,000 nm, about 5,000 nm, about 10,000 nm, about 50,000 nm, or about 100,000 nm. In some embodiments, the porous carbon network has an average pore size of at least about 10 nm, at least about 50 nm, at least about 100 nm, at least about 500 nm, at least about 1,000 nm, at least about 5,000 nm, at least about 10,000 nm, at least about 50,000 nm, or at least about 100,000 nm. In some embodiments, the porous carbon network has an average pore size of no more than about 10

nm, no more than about 50 nm, no more than about 100 nm, no more than about 500 nm, no more than about 1,000 nm, no more than about 5,000 nm, no more than about 10,000 nm, no more than about 50,000 nm, or no more than about 100,000 nm.

[0012] In some embodiments, the carbon network has a Raman spectrum with a D band at about 1323 cm^{-1}. In some embodiments, the carbon network has a Raman spectrum with a G-band at about 1570 cm^{-1}. In some embodiments, the carbon network has a Raman spectrum with a D' band at about 1604 cm^{-1}. In some embodiments, the carbon network has a Raman spectrum with a G'-band at about 2636 cm^{-1}. In some embodiments, the capacitor further comprises an amorphous carbon structure. In some embodiments, the amorphous carbon structure has a Raman spectrum with a D band at about 1324 cm^{-1}, In some embodiments, the amorphous carbon structure has a Raman spectrum with a D** band at about 1468 cm^{-1}. In some embodiments, the amorphous carbon structure has a Raman spectrum with a G band at about 1574 cm^{-1}. In some embodiments, the carbon network has a G' band spectrum curve with a full width at half maximum of about 74 cm^{-1}. In some embodiments, the carbon network is porous.

[0013] In some embodiments, the carbon network has an elemental composition of about 89% carbon, about 8% oxygen, and about 3% nitrogen. In some embodiments, the carbon network has an elemental composition of about 89% carbon, about 8% oxygen, and nitrogen. In some embodiments, the carbon network has an elemental composition of 89% carbon, 8% oxygen, and 3% nitrogen.

[0014] In some embodiments, the capacitor has a specific gravimetric capacitance of at least about 4 farads per gram (F/g), 5 F/g, 6 F/g, 8 F/g, 9 F/g, 10 F/g, 12 F/g, 15 F/g, or 20 F/g. In some embodiments, the capacitor has a specific gravimetric capacitance of about 4 F/g to about 20 F/g. In some embodiments, the capacitor has a specific volumetric capacitance of at least about 10 millifarads per cubic centimeter (mF/cm^3), 15 mF/cm^3, 20 mF/cm^3, 25 mF/cm^3, 30 mF/cm^3, 40 mF/cm^3, 50 mF/cm^3, or 60 mF/cm^3. In some embodiments, the capacitor has a specific volumetric capacitance of about 10 mF/cm^3 to about 60 mF/cm^3. In some embodiments, the capacitor has a capacitance after at least about 20,000 charge-discharge cycles of about 85%, 90%, 94%, 98%, or 99% of the initial capacitance. In some embodiments, the capacitor has a capacitance after at least about 20,000 charge-discharge cycles of about 85% to about 99% of the initial capacitance. In some embodiments, the capacitor has an equivalent series resistance of about 3 ohms to about 5 ohms. In some embodiments, the capacitor has an equivalent series resistance of at least about 3 ohms, at least about 4 ohms, or at least about 5 ohms. In some embodiments, the capacitor has an equivalent series resistance of at most about 3 ohms, at most about 4 ohms, or at most about 5 ohms.

[0015] Another aspect provided herein is a method for synthesizing a carbon network comprising: dissolving CNDs in a solvent to provide a CND slurry; casting the CND slurry onto a substrate; drying the CND slurry to provide a dry CND film; and irradiating the dry CND film with a light beam with a power level that is sufficient to convert at least a portion of the dry CND film into turbostratic graphene.

[0016] In some embodiments, the CNDs are irradiated at a predetermined temperature of about 200° C. to about 400° C. In some embodiments, the CNDs are irradiated at a predetermined temperature of at least about 200° C. In some embodiments, the CNDs are irradiated at a predetermined temperature of at most about 400° C. In some embodiments, the CNDs are irradiated for a predetermined time of about 1 hour to about 4 hours. In some embodiments, the CNDs are irradiated for a predetermined time of at least about 1 hour. In some embodiments, the CNDs are irradiated for a predetermined time of at most about 4 hours. In some embodiments, the solvent is an organic liquid. In some embodiments, the organic liquid is N-methyl-2-pyrrolidone (NMP).

[0017] In some embodiments, the CND slurry has a CND-to-NMP ratio of about 0.3:1 to about 0.9:1. In some embodiments, the CND slurry has a CND-to-NMP ratio of at least about 0.3:1, at least about 0.4:1, at least about 0.5:1, at least about 0.6:1, at least about 0.7:1, at least about 0.8:1, or at least about 0.9:1. In some embodiments, the CND slurry has a CND-to-NMP ratio of at most about 0.3:1, at most about 0.4:1, at most about 0.5:1, at most about 0.6:1, at most about 0.7:1, at most about 0.8:1, or at most about 0.9:1. In some embodiments, the CND slurry has a CND-to-NMP ratio of about 0.3:1 to about 0.4:1, about 0.3:1 to about 0.5:1, about 0.3:1 to about 0.6:1, about 0.3:1 to about 0.7:1, about 0.3:1 to about 0.8:1, about 0.3:1 to about 0.9:1, about 0.4:1 to about 0.5:1, about 0.4:1 to about 0.6:1, about 0.4:1 to about 0.7:1, about 0.4:1 to about 0.8:1, about 0.4:1 to about 0.9:1, about 0.5:1 to about 0.6:1, about 0.5:1 to about 0.7:1, about 0.5:1 to about 0.8:1, about 0.5:1 to about 0.9:1, about 0.6:1 to about 0.7:1, about 0.6:1 to about 0.8:1, about 0.6:1 to about 0.9:1, about 0.7:1 to about 0.8:1, about 0.7:1 to about 0.9:1, or about 0.8:1 to about 0.9:1. In some embodiments, the CND slurry has a CND-to-NMP ratio of about 0.3:1, about 0.4:1, about 0.5:1, about 0.6:1, about 0.7:1, about 0.8:1, or about 0.9:1.

[0018] In some embodiments, the light beam is generated by a laser. In some embodiments, the laser is a carbon dioxide laser. In some embodiments, the light beam has a power of about 8 W to about 13 W. In some embodiments, the light beam has a power of at least about 8 W, at least about 9 W, at least about 10 W, at least about 11 W, at least about 12 W, or at least about 13 W. In some embodiments, light beam has a power of at most about 13 W. In some embodiments, light beam has a power of about 12 W to about 13 W.

[0019] In some embodiments, the method further comprises synthesizing the CNDs from citric acid and urea, before dissolving the CNDs in the solvent. In some embodiments, the turbostratic graphene has an active surface area of at least about 230 square meters per gram (m^2/g). In some embodiments, the turbostratic graphene has an active surface area of at least about 100 m^2/g, at least about 120 m^2/g, at least about 140 m^2/g, at least about 160 m^2/g, at least about 180 m^2/g, at least about 200 m^2/g, at least about 220 m^2/g, at least about 240 m^2/g, at least about 260 m^2/g, at least about 280 m^2/g, or at least about 300 m^2/g. In some embodiments, the turbostratic graphene has an electrical conductivity of at least about 200 S/m. In some embodiments, the turbostratic graphene has an electrical conductivity of at least about 100 S/m, at least about 120 S/m, at least about 140 S/m, at least about 160 S/m, at least about 180 S/m, at least about 200 S/m, at least about 220 S/m, at least about 240 S/m, at least about 260 S/m, at least about 280 S/m, or at least about 300 S/m.

[0020] In some embodiments, the method produces a carbon network with a Raman spectrum having a D-band at

about 1323 cm^{-1}. In some embodiments, the method produces a carbon network with a Raman spectrum having a G-band at about 1570 cm^{-1}. In some embodiments, the method produces a carbon network with a Raman spectrum having a D' band at about 1604 cm^{-1}. In some embodiments, the method produces a carbon network with a Raman spectrum having a G'-band at about 2636 cm^{-1}. In some embodiments, the method produces an amorphous carbon structure with a Raman spectrum having a D band at about 1324 cm^{-1}. In some embodiments, the method produces an amorphous carbon structure with a Raman spectrum having a D** band at about 1468 cm^{-1}. In some embodiments, the method produces an amorphous carbon structure with a Raman spectrum having a G band at about 1574 cm^{-1}. In some embodiments, the carbon network has a G' band spectrum curve with a full width at half maximum of about 74 cm^{-1}.

[0021] In some embodiments, the porous carbon network has an average pore size of about 10 nm to about 100,000 nm. In some embodiments, the porous carbon network has an average pore size of at least about 10 nm. In some embodiments, the porous carbon network has an average pore size of at most about 100,000 nm. In some embodiments, the porous carbon network has an average pore size of about 10 nm to about 50 nm, about 10 nm to about 100 nm, about 10 nm to about 500 nm, about 10 nm to about 1,000 nm, about 10 nm to about 5,000 nm, about 10 nm to about 10,000 nm, about 10 nm to about 50,000 nm, about 10 nm to about 100,000 nm, about 50 nm to about 100 nm, about 50 nm to about 500 nm, about 50 nm to about 1,000 nm, about 50 nm to about 5,000 nm, about 50 nm to about 10,000 nm, about 50 nm to about 50,000 nm, about 50 nm to about 100,000 nm, about 100 nm to about 500 nm, about 100 nm to about 1,000 nm, about 100 nm to about 5,000 nm, about 100 nm to about 10,000 nm, about 100 nm to about 50,000 nm, about 100 nm to about 100,000 nm, about 500 nm to about 1,000 nm, about 500 nm to about 5,000 nm, about 500 nm to about 10,000 nm, about 500 nm to about 50,000 nm, about 500 nm to about 100,000 nm, about 1,000 nm to about 5,000 nm, about 1,000 nm to about 10,000 nm, about 1,000 nm to about 50,000 nm, about 1,000 nm to about 100,000 nm, about 5,000 nm to about 10,000 nm, about 5,000 nm to about 50,000 nm, about 5,000 nm to about 100,000 nm, about 10,000 nm to about 50,000 nm, about 10,000 nm to about 100,000 nm, or about 50,000 nm to about 100,000 nm. In some embodiments, the porous carbon network has an average pore size of about 10 nm, about 50 nm, about 100 nm, about 500 nm, about 1,000 nm, about 5,000 nm, about 10,000 nm, about 50,000 nm, or about 100,000 nm. In some embodiments, the porous carbon network has an average pore size of at least about 10 nm, at least about 50 nm, at least about 100 nm, at least about 500 nm, at least about 1,000 nm, at least about 5,000 nm, at least about 10,000 nm, at least about 50,000 nm, or at least about 100,000 nm. In some embodiments, the porous carbon network has an average pore size of no more than about 10 nm, no more than about 50 nm, no more than about 100 nm, no more than about 500 nm, no more than about 1,000 nm, no more than about 5,000 nm, no more than about 10,000 nm, no more than about 50,000 nm, or no more than about 100,000 nm.

[0022] In some embodiments, the carbon network has an elemental composition of carbon, oxygen, and nitrogen. In some embodiments, the carbon network has an elemental composition of about 89% carbon, about 8% oxygen, and about 3% nitrogen. In some embodiments, the carbon network has an elemental composition of about 89% carbon, about 8% oxygen, and nitrogen. In some embodiments, the carbon network has an elemental composition of 89% carbon, 8% oxygen, and 3% nitrogen. In some embodiments, the carbon network has an elemental composition of at least about 40% carbon. In some embodiments, the carbon network has an elemental composition of at least about 4% oxygen, at least about 5% oxygen, at least about 6% oxygen, at least about 7% oxygen, or at least about 8% oxygen.

[0023] Those skilled in the art will appreciate the scope of the present disclosure and realize additional aspects thereof after reading the following detailed description in association with the accompanying drawings.

BRIEF DESCRIPTION OF THE DRAWINGS

[0024] The accompanying drawing figures incorporated in and forming a part of this specification illustrate several aspects of the disclosure and, together with the description, serve to explain the principles of the disclosure.

[0025] FIGS. **1**A-**1**F show illustrations of an exemplary method of forming three-dimensional turbostratic graphene (3D-ts-graphene) from carbon nanodots (CNDs).

[0026] FIG. **1**A is an illustration of exemplary synthesized CNDs, in accordance with some embodiments.

[0027] FIG. **1**B is an illustration of exemplary thermolysis process of converting the CND to CND300, in accordance with some embodiments.

[0028] FIG. **1**C is an illustration of exemplary process of applying a CND300/NMP (N-methyl-2-pyrrolidone) slurry on a substrate, in accordance with some embodiments.

[0029] FIG. **1**D is an illustration of exemplary doctor blading apparatus, in accordance with some embodiments.

[0030] FIG. **1**E is an illustration of an exemplary process of evaporating NMP, in accordance with some embodiments.

[0031] FIG. **1**F is an illustration of exemplary process of laser-assisted conversion of CND300 into 3D-ts-graphene, in accordance with some embodiments.

[0032] FIG. **2** shows an image of an exemplary laser reaction chamber.

[0033] FIGS. **3**A-**3**E are characterization graphs of an exemplary thermolyzed CND (CND100-400), in accordance with some embodiments.

[0034] FIG. **3**A is a graph showing the percent weight loss of an exemplary CND sample at different treatment temperatures in the presence of oxygen or nitrogen, in accordance with some embodiments.

[0035] FIG. **3**B is an X-ray photoelectron C1s, N1s, and O1s spectra of an exemplary CND100-400, in accordance with some embodiments.

[0036] FIG. **3**C are Raman spectra of an exemplary CND100-400 upon excitation at a frequency of about 633 nm, in accordance with some embodiments.

[0037] FIG. **3**D is a powder X-ray diffraction pattern of an exemplary CND100-400, in accordance with some embodiments.

[0038] FIG. **3**E shows normalized Fourier-transform infrared spectroscopy spectra of an exemplary CND100-400, in accordance with some embodiments.

[0039] FIGS. **4**A-**4**C show images of an exemplary 3D-ts-graphene network (laser scribed CND300), in accordance with some embodiments.

[0040] FIG. **4**A is a scanning electron microscopy image of 3D-ts-graphene obtained at 3 kV, in accordance with some embodiments.

[0041] FIG. **4**B is a transmission electron microscopy image of a fragment of an exemplary 3D-ts-graphene at 120 kV, in accordance with some embodiments.

[0042] FIG. **4**C is a high-magnification transmission electron microscopy image of the edge of an exemplary 3D-ts-graphene fragment, in accordance with some embodiments.

[0043] FIG. **5**A shows a low-magnification scanning electron microscope (SEM) image of an exemplary graphite oxide sample that was laser-converted in argon at 3 eV, in accordance with some embodiments.

[0044] FIG. **5**B shows a high-magnification SEM image of an exemplary graphene oxide sample that was laser converted in argon at 3 eV, in accordance with some embodiments.

[0045] FIG. **5**C shows a higher magnification SEM image of an exemplary graphene oxide sample that was laser converted in argon at 3 eV, in accordance with some embodiments.

[0046] FIG. **5**D shows a low-magnification SEM image of an exemplary graphene oxide sample that was laser converted in oxygen at 3 eV, in accordance with some embodiments.

[0047] FIG. **5**E shows a high-magnification SEM image of an exemplary graphene oxide sample that was laser converted in oxygen at 3 eV, in accordance with some embodiments.

[0048] FIG. **5**F shows a higher magnification SEM image of an exemplary graphene oxide sample that was laser converted in oxygen at 3 eV, in accordance with some embodiments.

[0049] FIGS. **6**A and **6**B show measurement graphs of an exemplary 3D-ts-graphene network (laser scribed CND300), in accordance with some embodiments.

[0050] FIG. **6**A is a typical Raman spectrum of an exemplary 3D-ts-graphene obtained upon excitation at about 633 nm, in accordance with some embodiments.

[0051] FIG. **6**B is a X-ray photoelectron spectroscopy spectrum of an exemplary CND3001s with a zoom-in to the C1s peak, in accordance with some embodiments.

[0052] FIG. **7** shows Raman spectra of an exemplary laser-reduced graphene oxide lrGO reduced in argon and oxygen upon excitation at 633 nm, in accordance with some embodiments.

[0053] FIG. **8** shows Bode impedance plots of exemplary three double-layer capacitors coated with thin films of lrCND300(Ar), and lrCND300(O_2), in 0.1 M $TBAPF_6$/MeCN (tetrabutylammonium hexafluorophosphate/acetonitrile) as an electrolyte, in accordance with some embodiments.

[0054] FIG. **9** is an illustration of an exemplary photolytic mechanism of CND300.

[0055] FIGS. **10**A-**10**F show electrochemical data of an exemplary 3D-ts-graphene electrochemical capacitor with an electrolyte comprising 0.1 M $TBAPF_6$ solution in acetonitrile, in accordance with some embodiments.

[0056] FIG. **10**A is graph of material conversion versus laser power and conductivity versus laser power for an exemplary 3D-ts-graphene, in accordance with some embodiments.

[0057] FIG. **10**B are cyclic voltammograms an exemplary 3D-ts-graphene in an operative electrochemical window of 1.0 V at scan rates of 200, 500, and 1000 mV s^{-1}, in accordance with some embodiments.

[0058] FIG. **10**C are galvanostatic charge-discharge curves at different current densities of an exemplary 3D-ts-graphene, in accordance with some embodiments.

[0059] FIG. **10**D is specific gravimetric and areal capacitances of exemplary 3D-ts-graphene electrochemical capacitors with one or three sequentially applied layers, as a function of the scan rate, in accordance with some embodiments.

[0060] FIG. **10**E is Nyquist plot of exemplary 3D-ts-graphene electrochemical capacitors with one or three sequentially applied layers, in accordance with some embodiments.

[0061] FIG. **10**F is impedance phase angle versus frequency (Bode-plot) of exemplary 3D-ts-graphene electrochemical capacitors in comparison with a commercial activated carbon-based supercapacitor (Panasonic, 5.5 V/22 mF), in accordance with some embodiments.

[0062] FIG. **11** is a graph of volumetric specific energy and power densities of an exemplary 3D-ts-graphene cell with a 1.0 M tetrabutylammonium $TBAPF_6$/MeCN electrolyte, and of commercial energy storage devices, in accordance with some embodiments.

[0063] FIG. **12** is a diagram of an exemplary supercapacitor having electrodes comprising a carbon network, in accordance with some embodiments.

[0064] FIG. **13** is an illustration of an exemplary supercapacitor comprising a carbon network disposed onto flexible metal foil substrates with a flexible dielectric separator, in accordance with some embodiments.

DETAILED DESCRIPTION

[0065] The present disclosure provides a facile method for the conversion of biomolecule-based carbon nanodots (CNDs) into a carbon network comprising turbostratic graphene with a high surface area and excellent electrochemical properties. Further provided herein are carbon networks comprising turbostratic graphene and energy storage devices comprising the carbon network comprising turbostratic graphene.

[0066] Provided herein, per FIGS. **1**A-**1**F, is a method of converting CNDs into turbostratic graphene through thermolysis and laser treatment. FIG. **1**A is an illustration of exemplary synthesized CNDs. FIG. **1**B is an illustration of exemplary thermolysis process of converting the CND to CND300, in accordance with some embodiments. FIG. **1**C is an illustration of exemplary process of applying a CND300/NMP (N-methyl-2-pyrrolidone) slurry on a substrate, in accordance with some embodiments. FIG. **1**D is an illustration of exemplary doctor blading apparatus, in accordance with some embodiments. FIG. **1**E is an illustration of an exemplary process of evaporating NMP, in accordance with some embodiments. FIG. **1**F is an illustration of exemplary process of laser-assisted conversion of CND300 into three-dimensional turbostratic graphene (3D-ts-graphene), in accordance with some embodiments.

[0067] In some embodiments, the laser comprises an infrared laser. An exemplary laser treatment chamber is shown in FIG. **2**. The simple, cost-effective, and environmentally friendly method shown and disclosed herein is capable of readily producing high-performance electrodes with capabilities similar to those of graphene-based electrodes. In some embodiments, the method of converting CNDs into

turbostratic graphene employs the reaction of reduced CNDs in a CND/carbon dioxide (CO_2) plasma to form hierarchical porous networks of turbostratic graphene.

[0068] In some embodiments, the thermolysis is performed with small molecules. The small molecules may comprise, for instance, citric acid and urea. In some embodiments, the small molecule does not comprise graphite. In some embodiments, annealing is performed at temperatures up to about 400° C. The annealing may be performed in a tube furnace. Further, annealing may be performed in an oxygen-free environment. The method may further comprise applying CNDs on a substrate.

[0069] In some embodiments, the method comprises initially synthesizing the CNDs by microwave-assisted thermolysis and annealing. In some embodiments, the turbostratic graphene comprises a 3D-ts-graphene network. In some embodiments, the turbostratic graphene comprises a three-dimensional open porous turbostratic graphene network. The 3D-ts-graphene network exhibits excellent electrochemical properties, such as a critical hierarchical porous structure and a high surface area. For example, an exemplary 3D-ts-graphene network provided herein displays ideal capacitive behavior with a gravimetric capacitance of about 9.4 F g^{-1} a scan rate of 0.1 V s^{-1}, an energy density of about 7.5 Wh/kg at a power density of about 870 kW kg^{-1}, and an extremely fast charge-discharge cycling rate with a time constant of 1.05 ms. The 3D-ts-graphene network further exhibits an ideal morphology similar to graphene aerogels and graphene foam.

Thermolysis of CNDS

[0070] Carbon nanodots feature an extended π-system in their core and a variety of functional groups on their surface. Thermal treatment of CNDs induces the cleavage of some of these functional groups such as carboxylates, amides, and hydroxyl groups. Of particular interest is the decarboxylation, as it is typically accompanied with a reduction process.

[0071] In some embodiments, the as-synthesized CNDs were treated at elevated temperatures. In some embodiments, the as-synthesized CNDs were treated in a tube furnace. In some embodiments, the as-synthesized CNDs were treated in the absence of oxygen to modify their surface functionalities. Some embodiments further comprised employing a constant argon flow over the sample to ensure the transport of the outgassed material. In FIG. **3**A, the weight loss of CNDs when treated at different temperatures between 200° C. and 800° C. is shown. Notably, in the presence of oxygen in the carrier gas (air), the exemplary CNDs fully decompose at temperatures of about 500° C. In the absence of oxygen, a continuous weight loss from about 20% to about 60% is observed between about 200° C. and about 500° C., and a constant mass for thermolysis temperatures is observed between about 500° C. and about 800° C.

[0072] The reaction temperature and, subsequently, the material conversion are strongly dependent on the presence of oxygen as an oxidizer in the atmosphere. In the absence of oxygen, the functional groups from CND300 may be cleaved off and the remaining electrons in the carbon form a π-conjugated network. In the presence of oxygen, carbon is removed from the conjugated skeleton of the precursors, CND300, and carried away upon reaction with oxygen (O_2) in the form of CO_2.

[0073] Exemplary CND samples were prepared by annealing CNDs at different temperatures and are denoted herein by their annealing temperature, whereby, for example, CND300 represents CNDs annealed at about 300° C. In some embodiments, annealing at higher temperatures causes decreased solubility in polar solvents typically used for CNDs, such as water, dimethyl sulfoxide (DMSO), dimethylformamide (DMF), and N-methyl-2-pyrrolidone (NMP). For example, CND300 may be more soluble in DMSO, DMF, and NMP than in water. CND350 may only be soluble in the previously mentioned solvents in trace amounts even upon applying ultrasonication or heat, as shown in FIG. **3**A. In general, all CNDs are insoluble in nonpolar solvents such as toluene or chloroform.

[0074] FIG. **3**B shows exemplary X-ray photoelectron spectroscopy (XPS) spectra of thermolyzed CNDs, with emphasis on the C1s, N1s, and O1s regions. As seen, the increase in temperature may increase the carbon from about 57% to greater than about 70%, whereby intensity of the O1s peak gradually decreases, showing the elimination of oxygen-containing functional groups. Moreover, at temperatures greater than 300° C. the O1s peak visibly splits up into two separate peaks with maxima at about 530 eV and about 532 eV, which may show the transformation from —COH to C—O—C groups. According to the thermogravimetric analysis/mass spectrometry analysis, —OH and CO_2 may be the main leaving groups in this temperature region. A decrease in intensity may also be observed for the N1s peak at about 400 eV; however, at temperatures of greater than about 300° C., a second peak may evolve at about 400 eV. At the C1s region, in the temperature regime between about 100° C. and about 300° C., the oxygen bonded carbons, C—OH, C═O, and COOH, may continuously decrease in intensity. Notably, among these the COOH peak vanishes most significantly. Compared with the other peaks, the sp^2-hybridized carbon peak grows with increasing temperature on account of the sp^3-hybridized carbon peak and becomes dominant at temperatures greater than about 300° C.

[0075] The XPS data may show a conversion of functional groups and an increasing graphitization, that is, an increasing sp^2-hybridization upon thermolytic treatment of CNDs. With the elimination of the functional groups, in particular carboxylates, the solubility of the CNDs may decrease. A turning point from highly functionalized carbon dots to graphitized carbon dots occurs in the temperature range between about 300° C. and about 350° C.

[0076] Per FIG. **3**C, the Raman spectra of exemplary CNDs thermolyzed at temperatures of greater than about 300° C. are superimposed by background fluorescence, where peaks at about 1350 cm^{-1} and about 1600 cm^{-1} may be noticeable. At higher thermolytic temperatures, of greater than about 250° C., the fluorescence may vanish and the peaks may become more pronounced. Due to the small size of the conjugated π-systems, the D band may be very intense. Raman spectrum of CNDs between about 1000 cm^{-1} and about 1700 cm^{-1} comprise four peaks, namely the D*-, D-, D**-, and G-bands at about 1170 cm^{-1}, about 1350 cm^{-1}, about 1433 cm^{-1}, and about 1585 cm^{-1}. The D*- and D** bands may be found in amorphous carbon and nanocrystalline diamond or samples with CH_3-rich phases.

[0077] Upon annealing, the sp^3-carbon in hydrogenated carbon films transform into sp^2-carbon, whereby, with increasing thermolysis temperatures, the sp^3-signals, espe-

cially at about 1170 cm^{-1}, are found to gradually decrease. For example, CND200 shows a high intensity in the D* and D region, while for CND250 both the D* and D intensity may be significantly smaller. Since the D peak originates from a double resonant scattering process near defect sites, such as sp^3-carbons, its intensity is related to these signals.

[0078] As shown in the x-ray diffraction patterns in FIG. **3**D, only the long-range order of crystalline phases is detected, regardless of the presence of amorphous groups. In all samples, a peak in the 26° 2θ range is detected, where the graphitic (002) signal typically occurs, showing the presence of graphitic carbon in each sample. The exemplary samples may show a high degree of disorder, as the peak width is rather broad. In the lower temperature range between about 100° C. and about 300° C., the peaks sharpen with increasing temperature. At temperatures of greater than about 300° C., the peak broadens again and an additional broad peak at 11° 2θ evolves, which is the typical deflection angle originating from the (002) plane spacing of graphite oxide. This trend shows that with increasing temperature, the CND aggregates may gain order and a threshold is passed at which the long-range order in the material changes dramatically. These results suggest that highly disordered CNDs with a large proportion of sp^3-hybridized carbon convert into moderately ordered graphite-like materials with a large lattice spacing.

[0079] Per the Fourier-transform infrared spectroscopy (FT-IR) spectra in FIG. **3**E, the transformation of highly functionalized CNDs to a graphite-like material is also observable. All spectra were normalized at about 1840 cm^{-1} and about 1580 cm^{-1} to ensure comparability. The broad absorption maximizing at about 2793 cm^{-1} and about 3173 cm−1 are assigned to OH vibrations. A closer look reveals the presence of two peaks at about 3336 cm^{-1} and about 3443 cm^{-1} that are assigned to NH stretching vibrations. Both of these gradually disappear with higher thermolytic temperatures. A large bimodal peak with maxima at about 1578 cm^{-1} and about 1694 cm^{-1} originates from the C═C stretching vibrations of aromatic carbon and carbonyls (C═O) stemming from carboxylic acids, carboxylates, and amides. The peaks in the about 1000 cm^{-1} to about 1700 cm^{-1} region are typically assigned to oxidized functional groups such as C—OH, C—O—C, —C═O, and —COOH. For example, peaks at about 1046 cm^{-1} and about 1248 cm^{-1} are assigned to C—O—C(epoxides) and C—OH out-of-plane vibrations. The peaks at about 1144 cm^{-1} and about 1180 cm^{-1} may be related to either C—N stretching or C—O—C out-of-plane vibrations. The predominant absorptions of CND350 and CND400 appear at about 1578 cm^{-1} and 1046 cm^{-1}, where aromatic C═C and C—O—C stretching vibrations are resonant. Moreover, the C—H stretching vibrations at about 2850 cm^{-1} and about 2928 cm^{-1} are present in all samples with a similar intensity. A gradual elimination of functional groups like —OH, —NH and —COOH is reflected in the FT-IR spectra as the features related to these groups diminish with higher thermolytic temperatures. With respect to the x-ray diffraction peak at 11° 2θ for CND350 and CND400, which is typical for graphene oxide (002), the splitting of the O1s XPS signal and the FT-IR absorptions in the about 1000 cm^{-1} to about 1250 cm^{-1} region, it is assumed that oxygen bound in the form of epoxides remain between the layers of graphitic nanoparticles upon thermolysis at >300° C. Even in reduced graphene oxide these peaks still appear.

[0080] The nanographitic nature of these thermolyzed CND samples makes suitable precursors for conversion to large extended graphene networks. In general, solubility is an important criterion for the processability of the samples; however, the amount and the nature of the functional groups are decisive for their reactivity.

Laser-Induced Conversion

[0081] Exemplary films of CND300 were formed on different substrates, such as aluminum, copper, polyethylene terephthalate, or glass. A slurry of CND300 was prepared in NMP in a ratio of about 2:3 (CND300/NMP). The slurry may be applied on the substrate by doctor blading to achieve homogeneous films. The films were subsequently irradiated with an infrared laser, as shown in FIG. **1**F. Changes to the material are apparent to the naked eye, whereby a large part of the material is removed, and a changes in color from brownish to black occurs. In one example, up to about 60% of the initially cast CND300 material was removed. By contrast to non-irradiated CND300, the irradiated fraction may be insoluble in typical solvents such as DMSO, NMP, and DMF.

[0082] The change in morphology of the CND300 film upon laser irradiation is shown in the scanning electron microscopy (SEM) images presented in FIG. **4**A. The laser-irradiated CND300 film exhibits a spongy hierarchical porous structure with average pore sizes ranging from several tens of nanometers to tens of microns. In one embodiment, the carbon network is porous having average pore sizes that range from 10 nanometers (nm) to 100 nm. In another embodiment, the carbon network is porous, having average pore sizes that range from 100 nm to 500 nm. In yet another embodiment, the carbon network is porous, having average pore sizes that range from 500 nm to 1000 nm. In still another embodiment, the carbon network is porous, having average pore sizes that range from 1000 nm to 10,000 nm. In still yet another embodiment, the carbon network is porous, having average pore sizes that range from 10,000 nm to 100,000 nm.

[0083] Ultrathin layers of carbon are seen in the high-magnification images of an exemplary 3D-ts-graphene in FIG. **4**B. As seen, the pores are separated by carbon walls consisting of only a few layers of graphene. Moreover, the turbostratic nature, and the random orientation of the layers, is seen in the high-magnification transmission electron microscope (TEM) image in FIG. **4**C.

[0084] In the SEM images in FIGS. **5**A-**5**F the same principal structural features, with small differences, are observed independent of the reaction medium. More open pores are found on the surface of the laser-sintered lrCND300 in an oxygen atmosphere, per FIGS. **5**D-**5**F, than on the surface of the laser-sintered lrCND300 in an argon atmosphere, per FIG. **5**A-**5**C.

[0085] The exemplary 3D-ts-graphene exhibited an active surface area of about 230 m^2/g, determined by the dye adsorption method, which is in line with other open porous carbon networks such as graphene foam or aerographene. The TEM images of the exemplary CND300 sample show individual particles on the order of about a few nanometers and aggregated particles with sizes of about 50 nm.

[0086] Raman spectra were recorded at different spots of the sample, and are shown in FIG. **6**A, to form Raman maps. For the greater part of the film, a typical Raman pattern of turbostratic graphene is observed with the D-, G-, D'-,

D+D", G'-, and D+G bands at about 1131 cm^{-1}, 1582 cm^{-1}, 1617 cm^{-1}, 2461 cm^{-1}, 2655 cm^{-1}, and 2922 cm^{-1}. The G'-band was fitted with a single Lorentzian with a full width at half maximum (FWHM) of about 49 cm-^{1}. Ideal single, bilayer, or trilayer graphene shows either a single Lorentzian or a set of distinguishable Lorentzians with FWHM of about 24 cm^{-1} at about 2700 cm^{-1}. The high intensities of both the D- and the D'-bands may demonstrate the high amount of defect sites within the material. Considering the small size of the precursor materials, that is, CND300, the edge states may account for the majority of defect sites.

[0087] The graphenic nature of the laser-scribed CND300 is also reflected in the XPS spectrum in FIG. **6**B. The spectrum shows a strong signal in the C1s region and negligible signals in the N1s and O1s regions. Moreover, the C1s region was accurately fitted by a single Gaussian-Lorentzian peak maximizing at about 295.9 eV, which is assigned to C═C carbon. From the C1s, O1s, and N1s peak areas an elemental composition of 89% carbon, 8% oxygen, and 3% nitrogen was determined.

[0088] Additional evidence for the overall turbostratic graphene—like nature of the material comes from powder x-ray diffraction patterns. In comparison to CND300, the (002) peak is shifted from 26.9° to 26.0° 2θ, indicating a separation of the individual layers. Moreover, an additional shoulder at 22.8° and a tail down to about 15° appear, which is expected for rotationally displaced stacked graphene layers.

[0089] The Raman patterns of all samples show the same set of peaks, namely the D-, the G-, D', and G'-peak at ~1329, ~1578, ~1609, and ~2652 cm^{-1}, respectively, as seen in FIG. **7**. The intensities of the D and D'-bands relate to defects in the graphitic lattice. Notably, samples reduced under oxygen, lrCND300(O_2), show a significantly enhanced D-band, indicating a higher number of defects. A bathochromic shift of the G-band of 3 cm^{-1} from 1584 (lrCND300(O_2)) to 1581 cm^{-1} (lrCND300(Ar)) is noted, indicating an increase in electron density when turning from O_2 to Ar as a reaction medium.

[0090] FIG. **7** shows Raman spectra of an exemplary laser-reduced graphene oxide lrGO reduced in argon and O_2 upon excitation at 633 nm, in accordance with some embodiments. As seen, the G-band may be sensitive to electron doping and the size of the crystalline domains, whereby a downshift of the G-band originates either from a shift of electron density into the conduction band of graphene/graphite or a higher degree of crystallinity of the sp^2-phases in the graphitic sample. In undoped graphite the G-band is typically located at about 1580 cm^{-1}. The oxygen-containing functional groups provide electron trap states and withdraw electron density from the conjugated sp^2-network.

[0091] Considering the smaller size of CND300 as a starting material, the resulting 3D-carbon network is expected to exhibit a more nanocrystalline nature. The presence of O_2 during the reduction of lrCND300 may lead to higher reaction temperatures and a higher conversion ratio of oxy-functionalized carbon into sp^2-carbon, resulting in a lower number of oxy-defects and a higher crystallinity. The impact of oxygen in the reaction environment on the resulting materials properties of lrCND300 may not be discernable. In lrCND300(Ar) the sheet conductivity is slightly higher with a conductivity of about 295 S/m compared with lrCND300(O2) having a conductivity of about 248 S/m.

[0092] FIG. **8** shows Bode impedance plots of exemplary three double-layer capacitors coated with thin films of lrCND300(Ar), and lrCND300(O_2), in 0.1 M tetrabutylammonium hexafluorophosphate/acetonitrile (TBAPF_6/MeCN) as electrolyte, in accordance with some embodiments. The device performance in terms of capacitance, determined by cyclic voltammetry (CV) and frequency response, determined by electrochemical impedance spectroscopy, was measured in different electrolyte systems including a 6 M potassium hydroxide and 0.1 M TBAPF6/MeCN sealed symmetric capacitor assembly.

[0093] As seen, both supercapacitor assemblies with electrodes coated with thin films of lrCND300(O_2) and lrCND300(Ar) may show a purely capacitive behavior; however, the shape of the of the CV curve is more rectangular for lrCND300(Ar) than for lrCND300(O_2). With lrCND300(O_2) higher capacitance is achieved, and the polarization effect displays a higher maximum phase angle of about 84° for lrCND300(Ar) and about 79° for lrCND300(O_2). Significantly, low relaxation times of about 1.05 ms and about 1.95 ms were measured for lrCND300(Ar) and lrCND300(O_2), respectively. The frequency region for capacitive behavior is significantly higher for lrCND300(Ar) than for lrCND300(O_2) as a phase angle of about 78° at 120 Hz is reached in lrCND300(Ar) and only about 60° in lrCND300(O_2).

[0094] Visual inspection of the film displays a noticeable difference in the structures in the upper and the bottom layers, whereby, when the upper layer is scratched off, a brownish layer on the substrate remains, which contrasts with the soluble upper layer. Raman analysis of the bottom layer revealed that it may comprise unconverted CND300, whereby such a layer may be formed regardless of the substrate or the film thickness. An influence of the thermal conductivity of the substrate is ruled out, as the same results are obtained with different metal substrates, such as aluminum, gold, copper, or graphite, and with insulating substrates, such as polyethylene terephthalate, glass, or silicon dioxide. Based on these findings, a formation mechanism was hypothesized, as illustrated in FIG. **9**, which form a porous 3D-ts-graphene network upon irradiation of the CNDs with a high-power infrared laser beam.

[0095] When CND300 is applied on the substrate, the polar groups on the surface may bind to the substrate via coordinative or hydrogen bonding. Laser irradiation may induce a decarboxylation of the upper lying CNDs similar to other carbon oxide materials. As the carbon dioxide is removed from the CND periphery, a reduced CND core remains. These reduced CNDs, when not bonded to the substrate, are mobile and react with other reduced CNDs by forming new C—C bonds. As such, the reduced CNDs form together with the CO_2 a CND plasma and react in colder zones. The flux of the hot plasma enables the formation of a hierarchical porous structure. A confirmation of the postulated mechanism is shown in the typical pillar-like 3D-ts-graphene in the SEM images.

[0096] The quality and the conversion ratio from CND300 to 3D-ts-graphene depends strongly on the laser power and, subsequently, on the energy input. An array of exemplary CND300 films were irradiated at different laser powers and subsequently analyzed by Raman spectroscopy. In the low laser power regime between about 4 W and about 8 W, the Raman spectroscopy may show no evidence for 3D-ts-graphene but may additionally show a decrease in the

background fluorescence intensity, which may be attributed to the elimination of functional groups. At laser powers above about 8 W, CND300 is converted to 3D-ts-graphene. Notably, with increasing laser power the D- and G- peaks in the Raman spectra sharpen, and both defect-related peaks, namely, the D and D'-peak, considerably decrease in intensity. This shows a drastic improvement of the defect density in the converted 3D-ts-graphene. The bottom layer, however, remains in all samples unconverted. FIG. **10**A shows a graph of the weight percentage of an exemplary material converted by the laser and the weight percentage of material remaining in the film after photolysis, whereby higher laser power may convert and remove more material, conversion being achieved using laser power of greater than about 12 W.

[0097] CND300 can be converted into 3D-ts-graphene even in bulk quantities. In an exemplary method of converting CND 300 to 3D-ts-graphene even in bulk quantities, photolyzed product of CND300 powder was collected in a separate vial and washed with NMP several times to remove unreacted material. The Raman spectrum of the exemplary washed bulk powder sample showed superimposed signals of turbostratic graphene with sharp D-, G-, D', and G'-bands at about 1323 cm^{-1}, 1570 cm^{-1}, 1604 cm^{-1}, and 2636 cm^{-1} and an amorphous structure with broad D, D**, and G bands at about 1324 cm^{-1}, 1469 cm^{-1}, and 1574 cm^{-1}. The FWHM of the G' band in the exemplary bulk sample is about 74 cm^{-1}.

Electrochemical Characterization and Optimization

[0098] The hierarchical porous structure of the 3D-ts-graphene film enables a very high surface area that is accessible to solvents and electrolytes, whereby the electronic properties of the 3D-ts-graphene film are dependent on several parameters, including film thickness and laser power.

[0099] As shown in FIG. **10**A, the conductivity of the graphene film scales with both the laser power and the conversion ratio. The conductivity of the film may depend on the interconnection between the converted carbon dots (CND300), which may be achieved by better interconnection of reduced CND300 within the plasma. In general, higher conductivity is achieved using higher laser power, whereas, a maximum conductivity of about 2.13 S/cm (213 S/m) for a single layer is achieved at a power of at least about 16 W. Films produced with a laser power of below about 12 W may show a very high internal resistance, due to a large amount of unconverted material. As such, increased power produces better interconnections due to the greater conversion from CND300 to 3D-ts-graphene at higher local temperatures. From the Raman spectra of the exemplary CND300 sample, conversion of CND300 is effective at a laser power of greater than about 8 W, and the quality of the graphene increases with higher laser power, as the defect induced D- and the D'-bands decrease.

[0100] However, excessive laser power may remove more material, due to higher local temperatures in the CND plasma and subsequently reduce the overall performance. Therefore, a laser power of between about 12 W and about 20 W is optimal to produce high-quality films. In one example, the highest possible material conversion occurs with three irradiations at a power of 12.8 W.

[0101] The conductivity of the film was further increased by two orders of magnitude to 198 S/cm by sequentially laser converting two or more layers to ensure the filling of the trenches milled in the first layer.

[0102] Exemplary electrodes were fabricated with a mass loading of about 0.05 mg on an area of about 1.8 cm^2 (0.03 mg/cm^2) and tested under real conditions in sealed coin cells with an electrolyte of 0.1 M solution of TBAPF6 in acetonitrile. Reference measurements with 1.0 M sulfuric acid as an electrolyte were conducted.

[0103] The cyclic voltammogram of an exemplary 3D-ts-graphene electrode has a pseudo-rectangular shape, shown in FIG. **10**B, in an operating electrochemical window of 1 V, whereby the shape is retained at different scan rates between 0.1 V s^{-1} and 100 V s^{-1}. Using the TBAPF6 electrolyte in acetonitrile, this pseudo-rectangular shape was retained in a larger voltage range up to 2.5 V. In this larger voltage window, the specific gravimetric (Cm) and volumetric (CV) capacitances were calculated to be Cm=9.3 F g^{-1} and CV=31 mF cm^{-3} at a scan rate of 0.1 V s^{-1}. This preferred capacitive behavior is also reflected in the pseudo-triangular shape of the galvanostatic charge-discharge curves, plotted in FIG. **10**C, which is retained within a current density range between 50 A/g and 2000 A/g. After 20,000 cycles, the electrode retained about 94.6% of its capacitance. The gravimetric and areal capacitances as a function of the scan rate are shown in FIG. **10**D for two exemplary 3D-ts-graphene cells having an electrode with one layer of 3D-ts-graphene and another with three sequentially applied layers. Upon sequentially applying three layers, the areal capacitance increases by a factor of about 3, whereby the additional material filled into the laser-milled trenches of the first layer, decreasing the overall average pore size and thus increasing the areal capacitance.

[0104] A very small internal resistance drop of the three-layer cell of only about 0.02 V at a current density of 100 A g^{-1} is observed at the beginning of the discharge curves, from which is derived an equivalent series resistance of about 4.05Ω. This value is confirmed in the electrochemical impedance spectroscopy data shown in FIGS. **10**E and **10**F. The Nyquist plot in FIG. **10**E presents a direct comparison the two exemplary 3D-ts-graphene electrochemical capacitors with one or three sequentially applied layers for the frequency range between 100 kHz and 0.1 MHz. In both exemplary electrodes, no semicircles are observed in the high-frequency region, indicating essentially no charge-transfer resistance.

[0105] In FIG. **10**F the electrochemical impedance data of an exemplary three-layer 3D-ts-graphene cell are compared with a commercial activated carbon—based capacitor. Notable is the fast charge-discharge rate of the 3D-ts-graphene cell with a relaxation time of about 3.44 ms (291 Hz at a phase angle=45°). A gravimetric specific energy density of about 7.5 Wh/kg at a power density of about 864 kW/kg was determined. These values are comparable to other open porous carbon structures such as carbon foams and holey graphene. In terms of volumetric parameters, the cells exhibit good performance as demonstrated in the energy vs. power density plot in FIG. **11**. In comparison to a commercial aluminum-based capacitor, the 3D-ts-graphene cell has a similar charge-discharge rate but a much higher energy density.

[0106] Overall, the electrochemical cells based on 3D-ts-graphene electrodes show promising behavior for applications in supercapacitors, in particular, with regard to the simplicity of the preparation process. Improvements in

terms of capacitance are expected to be achievable by increasing the specific surface areas, which are low in comparison to values of 1405 m^2/g obtained for activated carbon.

[0107] FIG. **12** is a diagram of an exemplary supercapacitor having electrodes comprised of the carbon network of the present disclosure. FIG. **13** is an illustration of a realized supercapacitor fabricated in accordance with the present disclosure.

[0108] As such, provided herein are 3D-turbostratic graphene networks and methods of forming 3D-turbostratic graphene networks by combining thermolysis and infrared laser treatment of bottom-up synthesized carbon nanodots based on citric acid and urea, whereby increasing infrared temperature treatment removes the functional groups on the surface of the CNDs, and hydroxyls convert to epoxy groups. During subsequent laser treatment, the thermolyzed CNDs are converted to 3D-ts-graphene networks. The hierarchical porous network forms in the flux of a hot CND plasma containing reduced CNDs and CO_2, which both form upon decarboxylation of thermolyzed CNDs in the laser beam. Electrodes based on exemplary 3D-ts-graphene networks show promising capacitive performance with specific gravimetric capacitances of 9.37 F g^{-1} obtained at 0.1 V s^{-1}, tunable areal capacitances, and extremely fast charging rates with a relaxation time of 3.44 ms. The method herein of forming the three-dimensional graphene networks is simple and allows for the one-step fabrication of three-dimensional graphene materials using inexpensive small molecular precursors. Moreover, the laser-assisted technique enables the production of patterned surfaces with very small feature sizes that is currently under investigation for potential applications.

EXAMPLES

Example 1—Carbon Nanodot Synthesis

[0109] Citric acid (5 g) and urea (5 g) were dissolved in deionized water (7.5 mL). A beaker with the reaction mixture was heated in a domestic microwave (700 W) until the solvent was evaporated. The reaction conducted at different scales yields the same products. In all experiments the ratio between citric acid and urea was kept constant. The CNDs from this reaction were thermolyzed at different temperatures between 175° C. and 800° C. in a tube furnace. The reaction vessel, typically quartz or alumina, containing the as-synthesized CNDs, was placed in the center of the tube furnace. The furnace was heated to the final temperature with a heating rate of 6 K/min and kept at the final temperature for 2 h. A gas flow of argon, nitrogen, or air was used to remove gaseous reaction products.

Example 2—Electrode Fabrication

[0110] A laser-reaction chamber, per FIG. **2**, was fabricated comprising a gas inlet opposite to the gas outlet, and a two-inch zinc selenide window in the lid. A sample was placed in the center of the chamber. A CO_2 laser (10.6 μm) was emitted into the gas-reaction chamber through the window while a continuous gas current of 0.1 L/s was inserted into the gas inlet during the reaction.

Example 3—Electrode Fabrication

[0111] Carbon nanodots or thermolyzed CNDs (CND300) were dissolved in NMP to obtain highly viscous slurries with a CND/NMP ratio of 40/60. The slurry was cast onto the substrate by doctor blading. Next, the wet film was dried on a hotplate at 200° C. The dry film was irradiated with a 40 W CO_2 laser (10.6 μm) using a full spectrum laser engraver at different power settings. Two additional layers of CND300 were sequentially applied and laser-converted. Powder samples of laser-converted CND300 (3D-ts-graphene) were collected from the converted films in vials and washed with NMP. The solvent was added to the sample, the suspension was stirred for 30 min, and then the suspension was centrifuged. After centrifugation, the supernatant containing unreacted CND300 was removed and the precipitate was repeatedly washed until the supernatant was clear. Electrochemical capacitors were assembled in two-electrode configurations in coin cells with electrode diameters of 15 mm. The electrodes were fabricated either directly on stainless steel spacers, typically used in coin cells, or on aluminum foil. Alumina-coated polyethylene membranes were used as separators.

Example 4—Characterization

[0112] Fourier-transform infrared spectroscopy was conducted on a FT/IR-4100 FT-IR Spectrometer from Jasco with a single reflection ATR unit attached. X-ray diffraction patterns were recorded on a D8 Discover powder X-ray diffractometer from Bruker using CuKα radiation (λ=1.5406 Å). Raman spectra were recorded with a Renishaw InVia Raman Microscope in either individual spectrum mode or mapping mode. Scanning electron microscopy was conducted on a FEI Nova 230 Nano SEM with an electron acceleration voltage of 3 or 5 kV. Samples were prepared on conductive substrates, either aluminum or copper foil. Transmission electron microscopy was conducted on a T12 TEM from FEI at an acceleration voltage of 120 kV. Transmission electron microscopy samples were prepared by drop-casting 5 μL diluted dispersions of 3D-ts-graphene powder in ethanol onto Lacey-carbon supported TEM grids. X-ray photoelectron spectroscopy spectra were recorded using a Kratos Axis Ultra DLD spectrometer equipped with a monochromatic Al Kα X-ray source (hv=1486.6 eV). High-resolution spectra were calibrated using carbon tape (Ted Pella) with a known C1s binding energy of 284.6 eV. Raw data were processed using CasaXPS software (version 2.3.16). C1s spectra were fit using Gaussian-Lorentzian line-shapes for all spectral components except for the sp^2 C—C component, which was fitted with an asymmetric line shape to reflect the metallic character of the respective samples.

Example 5—Determination of the Active Surface Area

[0113] The active surface area of CND300 and 3D-ts-graphene was determined by the methylene blue adsorption method. In brief, certain amounts of CND300 or 3D-ts-graphene were stirred in solutions of methylene blue (MB) in deionized water with known concentrations for 24 h. The solutions were then centrifuged at 16 kG to remove any suspended material. The number of MB molecules adsorbed to the surface was calculated from the difference in absorption at 665 nm with respect to the reference solution. Every MB molecule is assumed to occupy 1.35 nm^2 of the active surface area. Activated carbon was used as a reference. For all experiments involving MB, polypropylene beakers and vials were used.

Example 6—Electrochemical Characterization

[0114] Electrochemical characterizations were carried out with a Biologic VMP3 electrochemical workstation. Conductivity measurements were performed with a laser converted film on a silicon substrate. Solution-based measurements were conducted with a three-electrode setup using an Ag/Ag+ reference electrode and a platinum wire counter electrode. Electrochemical capacitors were assembled in coin cells with electrode diameters of 15 mm and tested under sealed conditions. The volumetric capacitance (CV) and gravimetric capacitance (C_m) are as follows:

$$C_m = \frac{I}{m \cdot \left(\frac{dV}{dt}\right)}, \quad C_V = \frac{1}{V \cdot \left(\frac{dV}{dt}\right)} \tag{1}$$

or by integration of the CV curves according to the following formula:

$$C_m = \frac{\int IdV}{2vm(E_1 - E_0)}, \quad C_V = \frac{\int IdV}{2vV(E_1 - E_0)}, \tag{2}$$

where $\int I\,dV$ is the area of the CV curve between 0 V and 1 V, v is the scan rate in V s^{-1}, V is the volume of the electrodes in cubic centimeters, m is the mass of the active electrode material, and (E_1-E_0) is the potential scan window in volts. The specific gravimetric or volumetric energy densities were calculated according to the following:

$$E_m = \frac{C_m \cdot (\Delta V)^2}{2 \cdot 3600}, \quad E_V = \frac{C_V \cdot (\Delta V)^2}{2 \cdot 3600} \tag{3}$$

The specific gravimetric or volumetric power densities were obtained using the following:

$$P_m = \frac{E_m \cdot \left(\frac{dV}{dt}\right) \cdot 3600}{\Delta V}, \quad P_V = \frac{E_V \cdot \left(\frac{dV}{dt}\right) \cdot 3600}{\Delta V}. \tag{4}$$

[0115] Those skilled in the art will recognize improvements and modifications to the present disclosure. All such improvements and modifications are considered within the scope of the concepts disclosed herein.

Terms and Definitions

[0116] Unless otherwise defined, all technical terms used herein have the same meaning as commonly understood by one of ordinary skill in the art to which this disclosure belongs.

[0117] As used herein, the singular forms "a," "an," and "the" include plural references unless the context clearly dictates otherwise. Any reference to "or" herein is intended to encompass "and/or" unless otherwise stated.

[0118] As used herein, the term "about" refers to an amount that is near the stated amount by 10%, 5%, or 1%, including increments therein. As used herein, the term "about," when used in reference to a percentage, refers to a percentage within plus or minus 10%, 5%, or 1%, from the listed value, including increments therein.

[0119] As used herein, the term "carbonization" refers to a description for a myriad of complex processes occurring during the oxidation of biomaterials.

[0120] As used herein, the term "turbostratic graphene" refers to a graphene structure comprising a plurality of layers, having a relative rotation between at least two of the layers.

[0121] As used herein, the term "dielectric" refers to an electrical insulator that can be polarized by an applied electric field.

What is claimed is:

1. An energy storage device comprising:

a. a first electrode; and

b. a second electrode separated from the first electrode by a dielectric, wherein at least one of the first electrode and the second electrode comprises a carbon network comprising a turbostratic graphene, and wherein the energy storage device has a charge-discharge cycling rate time constant of at most about 8 milliseconds.

2. The energy storage device of claim **1**, wherein the carbon network is porous.

3. The energy storage device of claim **2**, wherein the carbon network has an average pore size of about 10 nanometers (nm) to about 10,000 nm.

4. The energy storage device of claim **3**, wherein the carbon network has an elemental composition of about 90% carbon, about 8% oxygen, and nitrogen.

5. The energy storage device of claim **1**, wherein at least one of the first electrode and the second electrode have an active surface area of at least about 100 square meters per gram.

6. The energy storage device of claim **1**, wherein at least one of the first electrode and the second electrode have an electrical conductivity of at least about 200 siemens per meter.

7. The energy storage device of claim **1**, having an energy density of at least about 3 watt-hours per kilogram at a power density of at least about 860 kilowatts.

8. The energy storage device of claim **1**, having a specific gravimetric capacitance of at least about 4 farads per gram.

9. The energy storage device of claim **1**, having a specific volumetric capacitance of at least about 30 millifarads per square centimeter.

10. The energy storage device of claim **1**, retaining at least about 94% capacitance after about 20,000 charge-discharge cycles.

11. A method for synthesizing a carbon network comprising:

a. dissolving carbon nanodots (CNDs) in a solvent to form a CND slurry;

b. casting the CND slurry onto a substrate;

c. drying the CND slurry on the substrate to form a CND film; and

d. irradiating the CND film with a light beam to convert at least a portion of the CND film into turbostratic graphene.

12. The method of claim **11**, wherein irradiating the CND film with the light beam is performed at a predetermined temperature in an oxygen-free environment for a predetermined time.

13. The method of claim **12**, wherein the predetermined temperature is about 200° C. to about 400° C. and wherein the predetermined time is about 1 hour to about 3 hours.

14. The method of claim **11**, wherein the solvent is an organic liquid.

15. The method of claim **14**, wherein the organic liquid is N-methyl-2-pyrrolidone (NMP).

16. The method of claim **15**, wherein the CND slurry has a CND-to-NMP ratio of about 40/60.

17. The method of claim **11**, wherein the light beam is generated by a laser.

18. The method of claim **17**, wherein the laser is a carbon dioxide laser.

19. The method of claim **17**, wherein the power level of the light beam is between about 8 watts (W) and about 13 W.

20. The method of claim **17** wherein the power level of the light beam is between about 12 W and about 13 W.

21. The method of claim **11**, further comprising synthesizing the CNDs from citric acid and urea before dissolving the CNDs in the solvent.

22. The method of claim **11**, wherein the turbostratic graphene has an active surface area of at least about 230 square meters per gram and an electrical conductivity of at least about 200 siemens per meter.

23. The method of claim **11**, wherein the carbon network is porous and has an average pore size of about 10 nanometers (nm) to about 100,000 nm.

24. The method of claim **11**, wherein the carbon network has an elemental composition of about 89% carbon, about 8% oxygen, and about 3% nitrogen.

25. A carbon network comprising turbostratic graphene having an active surface area of at least about 230 square meters per gram and an electrical conductivity of at least about 200 siemens per meter.

26. The carbon network of claim **25**, wherein the carbon network is porous and has an average pore size of about 10 nanometers (nm) to about 100,000 nm.

27. The carbon network of claim **25**, wherein the carbon network has an elemental composition of about 89% carbon, about 8% oxygen, and nitrogen.

* * * * *